Cou Iter

AEDC-TR-80-17

Evaluation of Critical Sting Length on a 7-deg Cone as Determined by Measurements of Dynamic Stability Derivatives and Base Pressure for Mach Numbers 0.2 through 1.3

Fred B. Cyran, Bob L. Uselton, and Ed J. Marquart
ARO, Inc.

January 1981

Final Report for Period September 26, 1979 – October 3, 1979

ARNOLD ENGINEERING DEVELOPMENT CENTER
ARNOLD AIR FORCE STATION, TENNESSEE
AIR FORCE SYSTEMS COMMAND
UNITED STATES AIR FORCE

NOTICES
When U. S. Government drawings, specifications, or other data are used for any purpose other than a definitely related Government procurement operation, the Government thereby incurs no responsibility nor any obligation whatsoever, and the fact that the Government may have formulated, furnished, or in any way supplied the said drawings, specifications, or other data, is not to be regarded by implication or otherwise, or in any manner licensing the holder or any other person or corporation, or conveying any rights or permission to manufacture, use, or sell any patented invention that may in any way be related thereto.
Qualified users may obtain copies of this report from the Defense Technical Information Center.
References to named commercial products in this report are not to be considered in any sense as an indorsement of the product by the United States Air Force or the Government.

This report has been reviewed by the Office of Public Affairs (PA) and is releasable to the National Technical Information Service (NTIS). At NTIS, it will be available to the general public, including foreign nations.

APPROVAL STATEMENT

This report has been reviewed and approved.

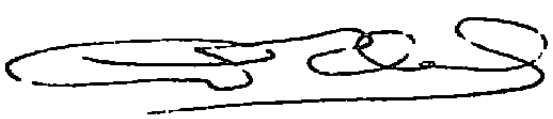

ALVIN R. OBAL, Captain, CF
Directorate of Technology
Deputy for Operations

Approved for publication:

FOR THE COMMANDER

JOHN M. RAMPY
Technical Director
Deputy for Operations

REPORT DOCUMENTATION PAGE		READ INSTRUCTIONS BEFORE COMPLETING FORM
1 REPORT NUMBER AEDC-TR-80-17	2 GOVT ACCESSION NO.	3 RECIPIENT'S CATALOG NUMBER
4 TITLE (and Subtitle) EVALUATION OF CRITICAL STING LENGTH ON A 7-DEG CONE AS DETERMINED BY MEASUREMENTS OF DYNAMIC STABILITY DERIVATIVES AND BASE PRESSURE FOR MACH NUMBERS 0.2 THROUGH 1.3		5 TYPE OF REPORT & PERIOD COVERED Final Report - Sept. 26, 1979 - Oct. 3, 1979 6 PERFORMING ORG REPORT NUMBER
7 AUTHOR(s) Fred B. Cyran, Bob L. Uselton, and Ed J. Marquart, ARO, Inc., a Sverdrup Corporation Company		8 CONTRACT OR GRANT NUMBER(s)
9 PERFORMING ORGANIZATION NAME AND ADDRESS Arnold Engineering Development Center/DOT Air Force Systems Command Arnold Air Force Station, Tennessee 37389		10 PROGRAM ELEMENT PROJECT, TASK AREA & WORK UNIT NUMBERS Program Element 65307F
11 CONTROLLING OFFICE NAME AND ADDRESS Arnold Engineering Development Center/DOS Air Force Systems Command Arnold Air Force Station, Tennessee 37389		12 REPORT DATE January 1981 13 NUMBER OF PAGES 56
14 MONITORING AGENCY NAME & ADDRESS(if different from Controlling Office)		15 SECURITY CLASS (of this report) UNCLASSIFIED 15a DECLASSIFICATION/DOWNGRADING SCHEDULE N/A

16 DISTRIBUTION STATEMENT (of this Report)

Approved for public release; distribution unlimited.

17 DISTRIBUTION STATEMENT (of the abstract entered in Block 20, if different from Report)

18 SUPPLEMENTARY NOTES

Available in Defense Technical Information Center (DTIC).

19 KEY WORDS (Continue on reverse side if necessary and identify by block number)

conical bodies	boundary layer transition
stability	Reynolds number
base pressure	angle of attack
wind tunnel tests	test methods
damping	

20 ABSTRACT (Continue on reverse side if necessary and identify by block number)

Wind tunnel tests were conducted to provide sting-support interference information for planning and directing wind tunnel tests at subsonic and transonic Mach numbers. Sting-length effects on dynamic stability derivatives, static pitching moment, and base pressure of a blunt, flat-base 7-deg cone were investigated at Mach numbers 0.2 to 1.3 in the Arnold Engineering Development Center (AEDC) Propulsion Wind Tunnel Facility (PWT). Two frequencies of oscillation, nominally 5.3 and 2.9 Hz, were investigated. The boundary-

DD FORM 1 JAN 73 1473 EDITION OF 1 NOV 65 IS OBSOLETE

20. ABSTRACT, Concluded.

layer state at the model base was turbulent for all Mach numbers greater than 0.2. The interference effects of two types of model-wake splitter plates were also investigated. The results showed that the critical sting length depended on the Mach number, angle of attack, and type of data used as the interference indicator. A critical sting length of three model diameters was determined to be suitable for all test conditions for the ratio of sting-diameter-to-model-base-diameter (0.22) for this test.

AFSC
Arnold AFS Tenn

PREFACE

The research reported herein was sponsored by the Arnold Engineering Development Center (AEDC), Air Force Systems Command (AFSC), Arnold Air Force Station, Tennessee. The results were obtained by ARO, Inc., AEDC Group (a Sverdrup Corporation Company), operating contractor for the AEDC. The work was done under ARO Project Numbers V32F-09A and P41C-A9. Mr. Alexander F. Money and Captain Alvin R. Obal (CF) were the Air Force Project Managers. The manuscript was submitted for publication on March 24, 1980.

CONTENTS

ILLUSTRATIONS

Figure | Page

TABLES

APPENDIXES

1.0 INTRODUCTION

Within the last few years, the demand for more accurate wind tunnel data has placed greater emphasis on the evaluation of sting-support interference effects. An understanding of support interference is necessary for an aerodynamicist to accurately predict full-scale flight vehicle characteristics based on wind-tunnel data. To obtain information on the evaluation of support interference effects, a continuing research program was initiated at the Arnold Engineering Development Center (AEDC) von Kármán Gas Dynamics Facility (VKF) in 1976; results of various tests supporting this research program up to the present are documented in Refs. 1 and 2. Support interference effects on dynamic stability and base-pressure measurements of a 7-deg cone at Mach number 3 are described in the 1976 work (Ref. 1). Efforts in 1977 and 1978 (Ref. 2) extended the 1976 work to Mach numbers 2 to 8 and investigated interference effects on base- and surface-pressure measurements of a 6-deg sliced-base cone. The 1979 work documented in this report extended the 7-deg cone investigation into the subsonic-transonic region; programs are planned at AEDC to extend this research to the testing of aircraft and missile configurations.

The 1979 research objective was to define critical sting lengths for a conical model in subsonic and transonic flow. Critical sting length is generally defined as the shortest sting length which does not change the level of an aerodynamic measurement obtained using longer stings. In this report the critical sting lengths were defined by the measurements of pitch-damping derivatives, static pitching moment, and base pressure.

The test model was a 15-percent spherically blunt 7-deg cone. Data were obtained at a model oscillation amplitude of ± 1 deg, using the forced-oscillation technique. Two oscillation frequencies, nominally 2.9 and 5.3 Hz, were tested, and data were obtained for angles of attack from 0 to 26 deg at Mach numbers from 0.2 to 1.3. The sting length was effectively varied from 1 to 3.4 model diameters by extending a conical flare to various stations along the sting. Based on model base diameter, the Reynolds number ranged from 0.2×10^6 to 3.6×10^6, and the reduced frequency parameter ($\omega D/2V$) varied from 0.006 to 0.048. The effects of two types of model-wake splitter plates were also investigated. The test was conducted in the Propulsion Wind Tunnel Facility (PWT), Aerodynamic Wind Tunnel (4T) from September 26, 1979 to October 3, 1979. The test data in this report are also documented in Ref. 3.

A summary and discussion of available reports dealing with support interference for general model configurations and tunnel conditions is presented in Ref. 1, and additional reports were added to this summary in Ref. 2. These summaries also indicate significant areas where critical sting-length data are not available. The results documented in this report

have been used to fill some of the voids in the "Suggested Sting Criteria" summaries of Refs. 1 and 2. A portion of the "Suggested Sting Criteria" is presented in Appendix A and includes the present results. Only that portion of the summary containing critical sting-length data for slender flat-base cones in the subsonic and transonic Mach regimes is presented in this report. Although an analysis of sting-length interference effects at subsonic and transonic Mach numbers on general model configurations is beyond the scope of this report, the results of this report should be applicable to most flat-base bodies of revolution in similar flow conditions.

Unless otherwise stated in this report, the term "interference" refers to sting-length interference effects only. Stings with lengths greater than the critical sting length are referred to as "noninterference" stings. The term "clean sting" denotes the maximum effective sting-length ratio (L_S/D) used in the present test (L_S/D = 3.3 or 3.4).

2.0 APPARATUS

2.1 TEST FACILITY

The Aerodynamic Wind Tunnel (4T) is a closed-loop, continuous-flow, variable-density tunnel in which the Mach number can be varied from 0.1 to 1.3 and can be set at discrete Mach numbers of 1.6 and 2.0 by placing nozzle inserts over the permanent sonic nozzle. Stagnation pressure can be varied from 400 to 3,400 psfa at all Mach numbers. The test section is 4 ft square and 12.5 ft long with perforated, variable-porosity (0.5- to 10-percent open) walls. It is completely enclosed in a plenum chamber from which the air can be evacuated, allowing part of the tunnel airflow to be removed through the perforated walls of the test section. The model support system consists of a sector and boom attachment which has a pitch angle capability of -7.5 to 28 deg with respect to the tunnel centerline and a roll capability of -180 to 180 deg about the sting centerline. A more complete description of the tunnel may be found in Ref. 4.

2.2 MODEL AND STING HARDWARE

The model was a flat-base 7-deg half-angle cone with a nose bluntness ratio (nose diameter-to-base diameter) of 15 percent. The moment reference axis was coincident with the model pivot axis at 60.9 percent of the model length aft of the model nose. Constructed of stainless steel, the model weighed 30.4 lb, and had a moment of inertia about the pivot axis of 0.408 slug-ft^2. Stainless-steel rings coated with Carborundum® grit and spot-welded to the model just behind the model nose were used as boundary-layer trips at some of the test conditions. Details of the model and boundary-layer trips are shown in Fig. 1.

When mounted to the test mechanism (described in Section 2.3 below), the model had an effective sting-length-to-model-diameter ratio (L_S/D) of 3.4 and an effective sting-diameter-to-model-diameter ratio of 0.22 (D_S/D) at the model base. The sting length was effectively shortened by positioning a conical flare (Fig. 2) at 1.0, 1.5, 2.0, 2.5, 3.0, or 3.3 model diameters to the rear of the model base along the sting. The flare was mounted to the motor housing without touching the sting forward of the motor housing. This mounting eliminated the possibility of the flare changing the sting frequency characteristics or model tare damping.

The two types of model-wake splitter plates which were attached to the conical flare are shown in Fig. 3, and plate installation details are shown in Fig. 4. A circular clamp was attached to minimize vibration at the forward end of the long plates (No. 8 Plates). Neither the clamp nor the plates touched the sting. The sting, conical flare components, and splitter plates were designed and built at AEDC and were also used during previous tests (Refs. 1 and 2). A sketch of the model installation is presented in Fig. 5. A photograph in Fig. 6 shows a typical model-sting configuration in the test section.

2.3 TEST MECHANISM

The VKF 1.C Forced-Oscillation Test Mechanism (Fig. 7) uses a cross-flexure pivot, an electric shaker motor, and a one-component moment beam instrumented with strain gages to measure the forcing moment of the shaker motor. The motor is coupled to the moment beam by a connecting rod and flexural linkage. The flexural linkage converts the translational force to a moment to oscillate the model at amplitudes up to ± 3 deg (depending on the balance flexure) and at frequencies from 2 to 8 Hz. The cross flexures are instrumented to measure the pitch/yaw displacement, support the model loads, and provide the restoring moment to cancel the inertia moment when the system is operating at its natural frequency. The moment beam is not subjected to the static loads and can be made as sensitive as required for the dynamic measurements. A pneumatic- and spring-operated locking device holds the model during tunnel startup and shutdown.

Two different sets of cross-flexure pivots were used to obtain data at the high and low oscillation frequencies. The high frequency (5.3 Hz) was the primary frequency of oscillation and was obtained with cross flexures having a stiffness of 466 ft-lb/rad. The low frequency (2.9 Hz) was obtained with cross flexures having a stiffness of 141 ft-lb/rad. The same moment beam was used throughout the entire test.The beam has a thickness of 0.046 in. and is capable of measuring a total moment of 9.8 in.-lb.

The cross-flexure pivot, moment beam, and flexural linkage assembly are supported by a long, slender cylindrical sting with a 1-deg taper. This sting is instrumented with strain gages to measure its static and oscillatory deflections in both the pitch and yaw plane.

2.4 INSTRUMENTATION

2.4.1 Forced-Oscillation Instrumentation

The forced-oscillation instrumentation (Ref. 5) uses an electronic analog system with precision electronics. The control, monitor, and data acquisition instrumentation are contained in a portable console that can be easily interfaced with the instrumentation of the various wind tunnels at AEDC. The control instrumentation can vary the oscillation amplitude of the model within the flexure limits. Oscillation amplitude is controlled by an electronic feedback loop which permits testing of both dynamically stable and unstable configurations. Data are normally obtained at or near the natural frequency of the model-flexure system; however, electronic resolvers in the instrumentation permit data to be obtained off-resonance.

All gages are excited by d-c voltage, and outputs are increased to optimum values by d-c amplifiers. Typical balance outputs from an oscillating model are composed of oscillatory components (OC) superimposed on static components (SC). These components are separated by band-pass and low-pass filters. The SC outputs are used to calculate the static moment coefficients and static sting deflections. The OC outputs are input to the resolver instrumentation and precise frequency measuring instrumentation. The resolvers use accurate electronic analog devices to process the OC signals and output d-c voltages. The output d-c voltages are proportional to the square of the oscillation amplitude, the in-phase and quadrature (90-deg out-of-phase) balance-forcing torque components, and the in-phase and quadrature sting moment components. These outputs are converted to digital signals by an analog-to-digital (A/D) converter, and the data are recorded for a period of time at a sample rate appropriate for the test.

2.4.2 Model Base-Pressure Instrumentation

Model base pressure was measured with a pressure transducer located on the tunnel plenum chamber wall. The location of the orifice with respect to the model and sting is shown in Fig. 8.

3.0 TEST DESCRIPTION

3.1 TEST CONDITIONS

A summary of the nominal test conditions at each Mach number is listed in Table 1. The test summary, Table 2, lists all configurations that were tested.

The reduced frequency parameter ($\omega D/2V$) at the high-oscillation frequency (5.3 Hz) ranged from 0.008 radians at Mach number 1.3 to 0.048 radians at Mach number 0.2. At the low-oscillation frequency (2.9 Hz) the range was from 0.006 radians at Mach number 0.9 to 0.026 radians at Mach number 0.2. The oscillation amplitude was ± 1 deg.

3.2 TEST PROCEDURES

After tunnel conditions and model attitude were established, the model was unlocked and brought to the oscillation amplitude by the Forced-Oscillation Control System. At each angle of attack, generally two data points were taken, and data were obtained over a 60-sec interval for each data point at approximately 200 samples per second.

An Automatic Model Attitude Positioning System (AMAPS) was used to control the model position. Before the test, a list of model angle-of-attack requirements was programmed into the AMAPS. After data were obtained at a given angle of attack, the AMAPS was manually activated, and the model was automatically pitched to the next angle of attack on the AMAPS list.

3.3 DATA REDUCTION

The time-wise balance and sting gage signals, and steady-state model attitude and base-pressure measurements were transmitted to a DEC-10 System Computer. Values of the balance and sting gage outputs were averaged by the computer and used to calculate the dynamic derivatives. Both the SC and OC sting gage outputs were used to correct the data for sting-bending effects. The method used to reduce the data is given in Refs. 5 and 6.

3.4 UNCERTAINTY OF MEASUREMENTS

In general, instrumentation calibrations and data uncertainty estimates were made using methods recognized by the National Bureau of Standards. Measurement uncertainty is a combination of bias and precision errors defined as

$$U = \pm(B + t_{95}S)$$

where B is the bias limit, S is the sample standard deviation, and t_{95} is the 95th percentile point for the two-tailed Student's "t" distribution, which for degrees of freedom greater than 30 is equal to 2.

Estimates of the measured data uncertainties for this test are given in Table 3a. Tunnel parameter data uncertainties were determined from in-place calibrations through the data recording system. Static load hangings on the Forced-Oscillation Mechanism simulated the range of loads and deflections anticipated during the test, and measurement errors were based on differences between applied loads and deflections and corresponding values calculated from the mechanism calibration. Load hangings to verify the sting and balance calibrations were made in the tunnel prior to the test.

Propagation of the bias and precision errors of measured data through the calculated data was made in accordance with Ref. 7. Uncertainties in the calculated tunnel parameters are given in Table 3b, and uncertainties in the dynamic parameters are given in Table 3c. The quoted uncertainties are based upon steady-state operation and do not account for the effects of the support boom vibrations and/or unsteady flow phenomena. In some instances the repeatability of the pitch-damping derivatives ($C_{m_q} + C_{m_{\dot{\alpha}}}$) was 15 to 20 percent instead of the quoted uncertainties.

The static stability derivative (local scope of the pitching moment curve, C_{m_α}) is proportional to the difference of the square of the model aerodynamic frequency and the square of the tare frequency. Since the frequency difference was less than 2 percent for the majority of the data, the estimated uncertainty in the static stability derivative was relatively large. In addition, the sting-oscillation corrections used in the reduction of the static stability derivative data were of the same magnitude or larger than the static stability derivative aerodynamic effects. For these reasons, the static stability derivative data are not presented.

4.0 RESULTS AND DISCUSSION

The results and discussion are presented by sections dealing with particular aspects of the test. Investigations which were incidental to the actual determination of sting-support interference effects will be presented first. Section 4.1 discusses an investigation of the model boundary-layer state and its bearing on support interference investigations. This section will be followed by a comparison of noninterference subsonic and transonic data with previously obtained supersonic and hypersonic data for this model (Section 4.2). Results pertaining directly to the determination of sting interference effects are discussed in Sections 4.3 through 4.5. These sections include the effects of Reynolds number, frequency, and angle of attack on measurements obtained at various effective sting lengths. Section 4.6 discusses the

evaluation of critical sting length. A comparison of critical sting-length data with previous test results and the results of a limited splitter-plate investigation are discussed in Sections 4.7 and 4.8, respectively.

4.1 BOUNDARY-LAYER INVESTIGATION

It is documented in Refs. 1 and 2 that support interference effects on some measurements are dependent on the type of boundary layer at the model base. At the beginning of the test, data were obtained at various Reynolds numbers and with two different boundary-layer trips at selected Mach numbers to determine their effects on the measured aerodynamic results. The determination of the state of the model boundary layer was made by comparing pitch-damping derivatives and base-pressure ratio data with and without trips at the different Reynolds numbers.

For supersonic and hypersonic Mach numbers, the effects of the state of the model boundary layer on pitch-damping derivatives and base pressure are well known. Typical variations of these two measurements with Reynolds number, obtained from Ref. 2 for the present model at Mach number 5, are shown in Fig. 9. An increase in damping was found when transition occurred near the model base. As the Reynolds number was increased, transition moved forward on the model and resulted in turbulent flow near the base. This caused the damping to decrease to about the same level as the laminar flow data. This known trend (Refs. 8 and 9) is shown by the dashed line in Fig. 9. The presence of a boundary-layer trip provided turbulent flow at lower Reynolds numbers. The base-pressure ratio showed a gradual decrease as transition moved upstream on the model and became relatively constant as fully turbulent flow was established. Similar trends of damping and base-pressure data for supersonic-hypersonic Mach numbers are also reported in Refs. 8 and 9.

In comparing boundary-layer transition effects at subsonic-transonic Mach numbers and at supersonic-hypersonic Mach numbers, it was assumed that some effect (although not necessarily similar) would occur in the damping and base-pressure data for a wide Reynolds number range or when trips were used. The results of a Reynolds number variation and the effects of boundary-layer trips are shown in Fig. 10 for Mach numbers 0.2, 0.95, and 1.3. This investigation of the model boundary layer was conducted with the clean sting ($L_S/D \geq 3.3$) configuration and at zero angle of attack. At Mach numbers 0.95 and 1.3, both the pitch-damping derivatives and base-pressure ratio were essentially invariant with Reynolds number. The addition of the boundary-layer trips had virtually no effect on either measurement. Some effects of Reynolds number on the damping data were found at Mach number 0.2 at the lower Reynolds numbers. A similar effect at Mach number 0.2 was

reported in Ref. 10 for a 3-caliber secant-ogive cylinder. The base-pressure data obtained at M = 0.2 were not useful for indicating transition because the base-pressure ratio was very close to unity and no effect could be detected.

The primary tunnel conditions presented in Table 1 were chosen such that turbulent flow at the model base could be confidently assumed. However, a posttest analysis of the data in Fig. 10 indicated some doubt about the model boundary-layer state for the primary test condition at Mach number 0.2. Since sufficient data were not obtained for determining the model boundary-layer state at M = 0.2 and $Re_D = 0.3 \times 10^6$ (primary test condition), the model boundary layer at this condition is considered unknown. It was concluded from Fig. 10 that at all primary test conditions other than at Mach number 0.2, the boundary layer near the model base was turbulent. Further effects of Reynolds number on sting-length interference will be discussed in Section 4.3.

4.2 EXPERIMENTAL DATA COMPARISON

Pitch-damping derivative and base-pressure ratio data obtained during the present test at subsonic and transonic Mach numbers were combined with previously obtained supersonic and hypersonic Mach number data from Refs. 1 and 2 and plotted versus Mach number in Fig. 11. All data in Fig. 11 are for the present model mounted on the noninterference sting configuration ($L_S/D \geq 3.0$) with a turbulent boundary layer near the model base. This plot illustrates the variation of the noninterference data over the subsonic-hypersonic range. The data obtained from the present test are in good agreement with the extrapolated results from previously obtained supersonic and hypersonic data. These trends are expected for a slender cone.

4.3 EFFECT OF REYNOLDS NUMBER

At all primary Mach numbers (M = 0.2, 0.6, 0.9, 1.1, and 1.3), data were obtained at two Reynolds numbers for selected sting-length ratios to determine if Reynolds number affected the data for various interference-producing sting lengths. Figure 12 shows pitch-damping derivatives, the parameter $\Delta^i C_{m_\alpha}$ (see Section 4.5), and base-pressure ratio data as a function of effective sting-length ratio for two Reynolds numbers at Mach number 1.3. The boundary layer at the model base was turbulent for all conditions shown. The results in Fig. 12 are typical of the results at all other Mach numbers. In general, Reynolds number effects were not found on data obtained at various effective sting lengths.

4.4 EFFECT OF FREQUENCY

At Mach numbers 0.2, 0.6, and 0.9, data were obtained at two frequencies of oscillation to determine if the data obtained with various effective sting lengths were dependent on frequency. A typical comparison of pitch-damping derivatives as a function of angle of attack for two reduced frequencies is shown in Fig. 13. The data are for both the interference ($L_S/D = 1.0$) and clean ($L_S/D = 3.3$) sting configurations at Mach number 0.9. No effects of frequency were found for the Mach number and frequency range investigated.

4.5 EFFECT OF ANGLE OF ATTACK

Pitch-damping derivatives, the parameter $\Delta^i C_{m_\alpha}$, static pitching moment, and base-pressure ratio data as a function of angle of attack for various effective-sting-length ratios are presented in Fig. 14 for Mach numbers 0.2 to 1.3. The change in the static stability derivative attributable to interference, $\Delta^I C_{m_\alpha}$ (see Appendix B for the definition of $\Delta^i C_{m_\alpha}$), was found to be representative of the measurement of C_{m_α} in determining critical sting length. Unless otherwise noted, all discussions on interference effects on the static stability derivative C_{m_α} are based on the parameter $\Delta^i C_{m_\alpha}$. The parameter $\Delta^i C_{m_\alpha}$ and base-pressure ratio data are not presented at Mach number 0.2 because the relatively large uncertainty in the tunnel conditions at this point (see Table 3) resulted in excessively large uncertainties in $\Delta^i C_{m_\alpha}$. Also at Mach number 0.2, the base-pressure ratio was essentially unity, and base-pressure interference effects could not be accurately discerned. A review of the data in Fig. 14 shows that, in general, the interference effects on all measurements are smaller at high angles of attack than at low angles of attack. Figure 14 also shows that the angle-of-attack effect is influenced by Mach number. The damping data at $M = 0.6$ (Fig. 14b) for the interference sting configuration ($L_S/D = 1.0$) do not appear to approach the level obtained with the noninterference configuration ($L_S/D = 3.3$) as abruptly as the damping data at $M = 1.3$ (Fig. 14e) for increasing angles of attack. The static pitching-moment data generally exhibited sting-length dependence over the angle-of-attack range, except for Mach numbers greater than 1.0. Although interference effects generally decrease as angle of attack increases, Fig. 14 indicates that the dynamic measurements ($C_{m_q} + C_{m_{\dot\alpha}}$ and $\Delta^I C_{m_\alpha}$) may, in some instances, have slightly greater interference effect in the angle-of-attack range $0 < \alpha \leq 12$ deg than at $\alpha = 0$ for Mach numbers less than 1.10.

It is evident in Fig. 14 that interference effects are statically de-stabilizing at all Mach numbers. At Mach numbers less than or equal to 0.9, interference was dynamically de-stabilizing while at Mach numbers 1.1 and greater, the opposite was found. In all cases, interference caused an increase in the base-pressure ratio.

4.6 EVALUATION OF CRITICAL STING LENGTH

Damping derivatives, the parameter $\Delta^i C_{m_\alpha}$, and base-pressure ratio data are shown in Fig. 15 as a function of effective sting-length ratio for Mach numbers 0.2 to 1.3 for $\alpha = 0$ (only damping data are shown for Mach number 0.2). An arrow indicating the critical sting-length ratio (L_{cr}/D) is shown on each plot in Fig. 15, except for the plot of the parameter $\Delta^i C_{m_\alpha}$ at Mach number 0.9 (Fig. 15c) which is inconclusive. This exception indicates that the measurement of $\Delta^i C_{m_\alpha}$ at Mach number 0.9 may yield an erroneous value of L_{cr}/D based on data at $\alpha = 0$. However, Fig. 14c indicates that interference based on $\Delta^i C_{m_\alpha}$ data in the range $0 < \alpha < 12$ deg at Mach number 0.9 is present for an effective sting-length ratio of 1.5. For all data presented in Fig. 15, with the exception of the case mentioned above, a relatively constant measurement level is found for effective sting-length ratios greater than or equal to 3.0. The constant measurement level changes abruptly at some effective sting-length ratio in the range 1.0 to 3.0, depending on the Mach number and measurement. For all data presented in Fig. 15, critical sting-length ratios determined from the measurement of base pressure are always greater than or equal to the value of L_{cr}/D determined from the damping derivatives or the paramenter $\Delta^i C_{m_\alpha}$. Note in Fig. 15b that the critical sting length determined by the damping measurement at Mach number 0.6 is 1.5 model diameters. But the data in Fig. 14b indicate that, at Mach number 0.6 for angles of attack greater than zero, an L_S/D of 1.5 exhibits some interference effects. Therefore, the data in both Figs. 14 and 15 should be considered together for the best assessment of interference.

4.7 CRITICAL STING-LENGTH COMPARISON

The data in Figs. 14 and 15 were used to determine critical sting length, and the results are plotted in Fig. 16 as a function of Mach number. A dashed line in the $\Delta^i C_{m_\alpha}$ measurement plot indicates that data at angles of attack greater than zero were considered in the determination of critical sting length. Based on the data in Fig. 14, critical sting length as determined by the C_m measurement is certainly in the range $1.5 \leq L_{cr}/D \leq 3.3$, as shown in the shaded area in Fig. 16. A more precise determination of the critical sting length could not be made in this area because of insufficient data; however, the dashed line for the C_m measurement in Fig. 16 represents the author's estimate. Also shown in Fig. 16 are the results of Refs. 1 and 2, to depict the variation of critical sting length over the subsonic to hypersonic range for a turbulent boundary layer.

A review of Fig. 16 shows that a critical sting length of two model diameters is suitable over the Mach number range 0.2 to 5.0 for the measurement of damping derivatives. For the measurement of the pitching moment slope, a critical sting length of 2.5 model diameters is required for the Mach number range 0.6 to 0.9, and 2 model diameters is required for the

Mach number range 1.1 to 3.0. The critical sting length determined by the measurement of the static pitching moment varies from two model diameters at Mach number 0.2 to one model diameter at Mach numbers greater than 1.1. The measurement of base pressure indicates that a critical sting length of two to three model diameters is required.

Based on the data in Fig. 16, (turbulent boundary layer) a critical sting length of three model diameters is satisfactory regardless of the type of measurement. Base pressure, which has been used as an interference indicator for many years, seems to indicate the longest critical sting length compared to all other measurements previously investigated. Thus, static pitching moment and pitch-damping derivatives should be free from sting-length interference effects for sting lengths greater than or equal to the critical sting length determined by base-pressure measurements.

Critical sting-length data from other reference sources were sought to compare with the critical sting-length data determined from the present investigation. Only one critical sting-length evaluation (Ref. 11) on damping derivative measurements at subsonic-transonic speeds for a blunt, flat-base cone was found. Reference 11 reported no sting length effects for a blunt, flat-base cone (e.g. $L_{cr}/D = 0$) at Mach numbers 0.65 and 1.0. Discussion of Ref. 11 data is included in Refs. 1 and 12. Reference 1 states that the Ref. 11 data should be used with caution because the interference hardware used may have affected the measurements. Reference 12 states that the interference results were not representative of turbulent flow over the model base and that the Ref. 11 data were influenced by transition-amplified interference effects.

A substantial amount of critical sting-length data for base-pressure measurements for similar tests was found. Figure 17 presents critical sting-length data from various sources (Refs. 13, 14, and 15) combined with the present data for Mach numbers 0.6 to 2.4. It is evident in Fig. 17 that critical sting length for the measurement of base pressure is highly dependent on sting-diameter-to-model-base-diameter ratio (D_S/D) and flare angle (θ_s) in the subsonic and transonic range. In the supersonic region, ($M \geq 1.6$), the parameters D_S/D and θ_s do not appear to affect critical sting length significantly. In Fig. 17a, the critical sting length data for $\theta_s = 15$ deg in the subsonic region (present data) are lower than all other data, probably because of the relatively small value of D_S/D (0.22) compared to the data from the other sources ($D_S/D = 0.5$). Although only one value of D_S/D was used for the present test, it appears that this value ($D_S/D = 0.22$) did provide a negligible or minimal (within the measurement uncertainty) interference effect.

4.8 EFFECT OF SPLITTER PLATES ON INTERFERENCE

A limited investigation of splitter-plate effects on interference was conducted at Mach numbers 0.2, 0.6, and 0.9. In Fig. 18 damping derivatives, static pitching moment, and base-pressure ratio data are presented as a function of angle of attack for the two splitter plates tested at Mach number 0.9. Splitter-plate effects in Fig. 18 for Mach number 0.9 are typical of the effects at Mach numbers 0.2 and 0.6. Essentially no effects attributable to the presence of either splitter plate were found at all conditions tested.

5.0 CONCLUDING REMARKS

Sting interference effects as determined by the measurement of dynamic stability derivatives, static pitching moment, and base pressure were investigated at Mach numbers 0.2 through 1.3. The boundary layer at the model base for all Mach numbers greater than 0.2 was turbulent. Additional variables included angle of attack, frequency of oscillation, and the addition of splitter plates located behind the model. Data were obtained on a flat-base 7-deg cone with a spherical nose bluntness of 15 percent. Reynolds number, based on model base diameter, ranged from 0.2×10^6 to 3.6×10^6. The evaluation of critical sting length (the shortest sting length which does not change the constant measurement level obtained by longer stings) for a slender, flat-base cone at subsonic and transonic speeds is summarized in Appendix A. Conclusions based on these results are given below:

1. Critical sting length is dependent on the parameter selected as the interference indicator.
2. Critical sting length as determined by the measurement of pitch-damping derivatives and static pitching moment at subsonic to transonic speeds is less than or equal to 2 model diameters.
3. Critical sting length as determined by the measurement of the pitching-moment slope (C_{m_α}) is 2.5 model diameters at subsonic and transonic speeds.
4. Critical sting length as determined by the measurement of base pressure is generally 3 model diameters for Mach numbers 0.6 to 1.3.
5. Critical sting length determined by base-pressure measurements was found to be greater than or equal to the critical sting length determined by the aerodynamic coefficients.
6. Critical sting length was found to be independent of Reynolds number and frequency of oscillation.

7. In general, the addition of splitter plates behind the model had no effect on any measurements for the Mach number range (0.2 to 0.9).

8. The evaluation of critical sting length for a slender, flat base cone at subsonic and transonic speeds is summarized in Appendix A.

REFERENCES

1. Uselton, Bob L. and Cyran, Fred B. "Critical Sting Length as Determined by the Measurement of Pitch-Damping Derivatives for Laminar, Transitional, and Turbulent Boundary Layers at Mach Number 3 for Reduced Frequencies of 0.0033 and 0.0056." AEDC-TR-77-66 (AD-A042 747), July 1977.

2. Uselton, Bob L. and Cyran, Fred B. "Sting Interference Effects as Determined by Measurements of Dynamic Stability Derivatives, Surface Pressure, and Base Pressure for Mach Number 2 through 8." AEDC-TR-79-89, 1980.

3. Cyran, Fred B. "Sting Interference Effects on a 7-deg Cone as Determined by Measurements of Dynamic Stability Derivatives and Base Pressure for Mach Numbers 0.2 through 1.3." AEDC-TSR-79-P75, December 1979.

4. *Test Facilities Handbook* (Eleventh Edition). "Propulsion Wind Tunnel Facility, Vol. 4." Arnold Engineering Development Center, June 1979.

5. Burt, Glen E. "A Description of a Pitch/Yaw Dynamic Stability, Forced Oscillation Test Mechanism for Testing Lifting Configurations." AEDC-TR-73-60 (AD762286), June 1973.

6. Schueler, C. J., Ward, L. K., and Hodapp, A. E., Jr. "Techniques for Measurement of Dynamic Stability Derivatives in Ground Test Facilities." AGARDograph 121 (AD669227), October 1967.

7. Thompson, J. W., Jr. and Abernethy, R. B. et al. "Handbook Uncertainty in Gas Turbine Measurements." AEDC-TR-73-5 (AD755356), February 1973.

8. Uselton, Bob L. "Investigation of Sting Support Interference Effects on the Dynamic and Static Stability Characteristics of a 10-deg Cone at Mach Numbers 2.5, 3.0, and 4.0." AEDC-TDR-64-226 (AD450660), November 1964.

9. Ward, L. K. "Influence of Boundary-Layer Transition on Dyanamic Stability at Hypersonic Speeds." Transactions of the Second Technical Workshop on Dynamic Stability Testing, Vol. 11, Paper 6, Arnold Engineering Development Center, 1965.

10. Uselton, Bob L., and Shadow, Tom O. "Dynamic Stability Characteristics of 3- and 5-Cal Army-Navy Spinner Projectiles at Mach Number 0.2 through 1.3." AEDC-TR-70-115 (AD871403), July 1970.

11. Wehrend, W. R., Jr. "An Experimental Evaluation of Aerodynamic Damping Moments of Cones with Different Centers of Rotation." NASA TN-D-1768, March 1963.

12. Ericsson, Lars E. "Modification of Aerodynamic Prediction of the Longitudinal Dynamics of Tactical Weapons." LMSC-D646354, (Appendix) August 1979.

13. German, R. C. "Strut Support Interference on a Cylindrical Model with Boattail at Mach Numbers from 0.6 to 1.4," AEDC-TR-76-40 (AD-A024 473), May 1976.

14. Lee, George, and Summers, James L. "Effects of Sting-Support Interference on the Drag of an Ogive-Cylinder Body with and without a Boattail at 0.6 to 1.4 Mach Number." NACA RM-A57I09, December 1957.

15. Love, Eugene S. "A Summary of Information on Support Interference at Transonic and Supersonic Speeds." NACA-RM-L53K12, January 1954.

16. Rie, H., Linkiewicz, E. A., and Bosworth, F. D. "Hypersonic Dynamic Stability, Part III -Unsteady Flow Field Program," FDL-TDR-64-149, January 1967.

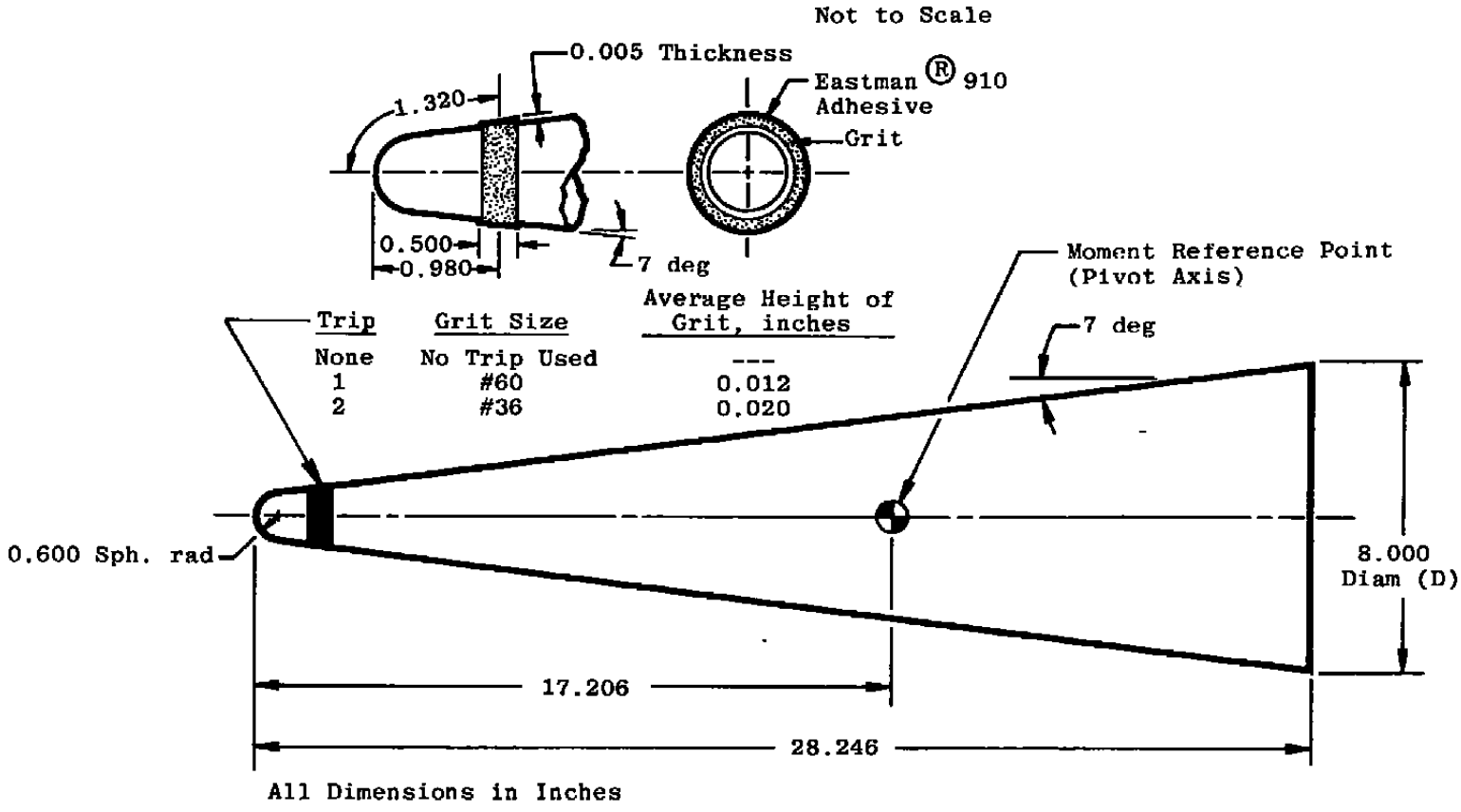

Figure 1. Details of model.

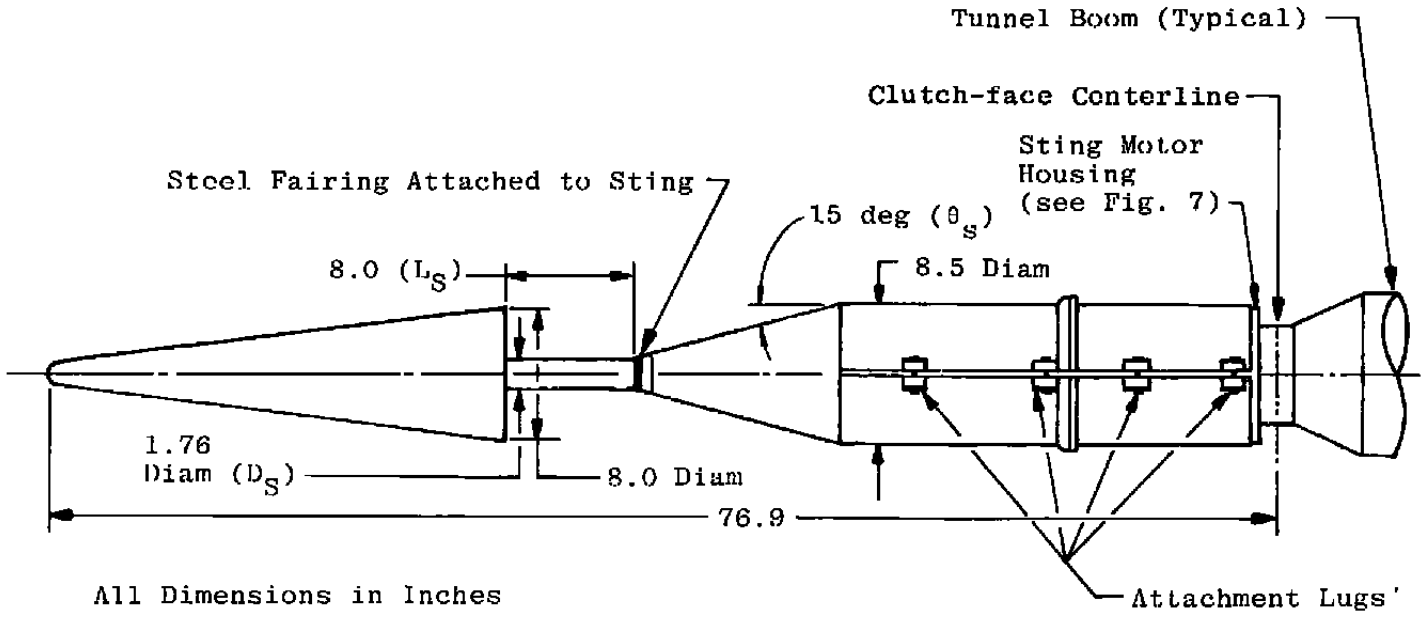

a. Interference sting, $L_S/D = 1.0$

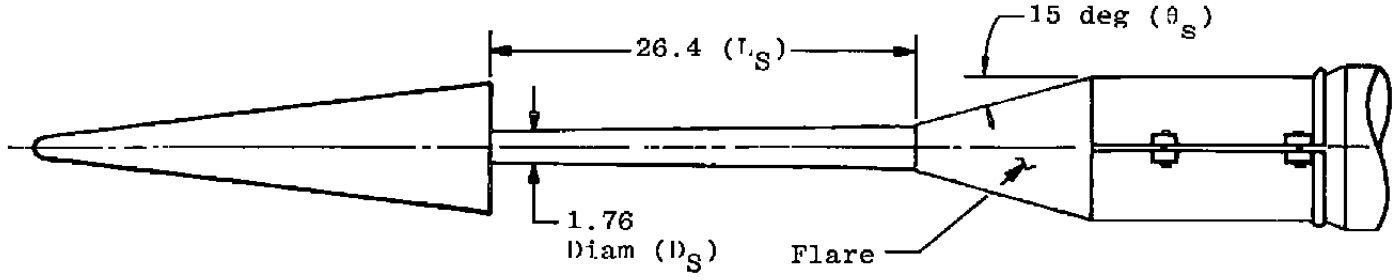

b. Clean sting, $L_S/D = 3.3$

Figure 2. Details of model support configurations.

All Dimensions in Inches

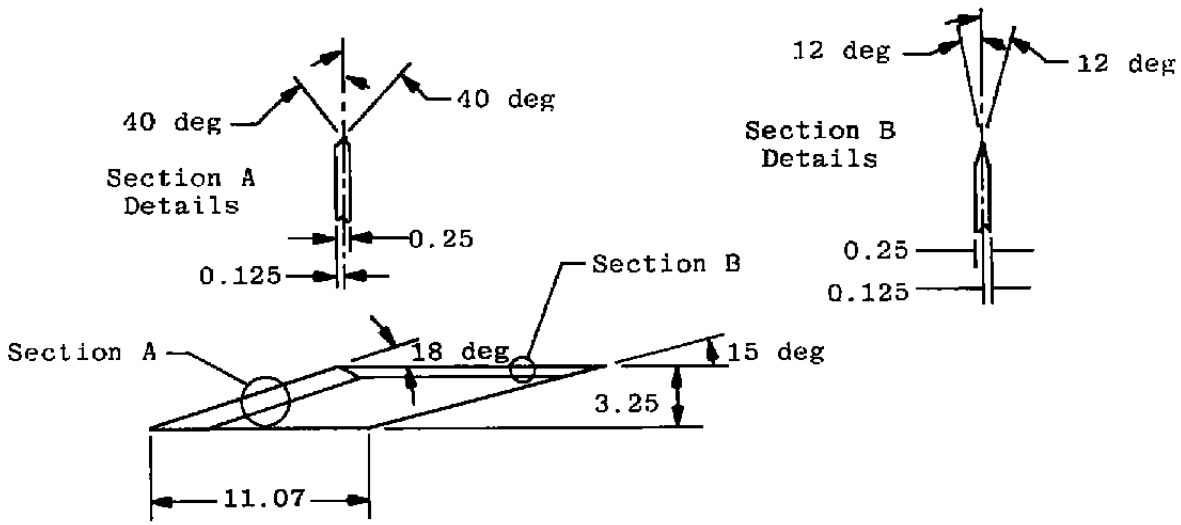

a. Plate 1

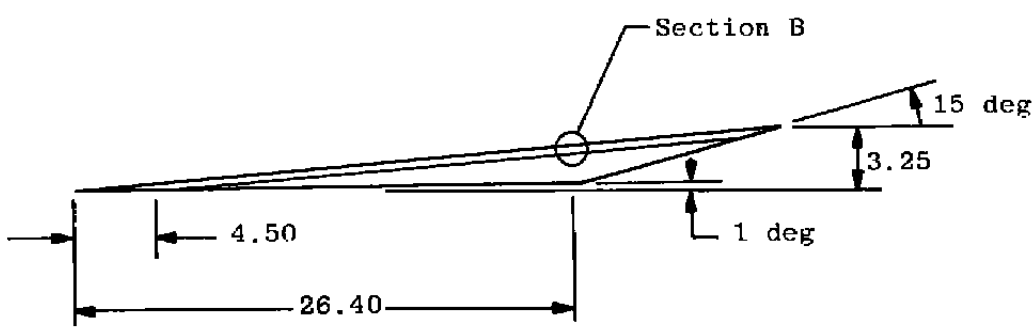

b. Plate 8

Figure 3. Details of splitter plates.

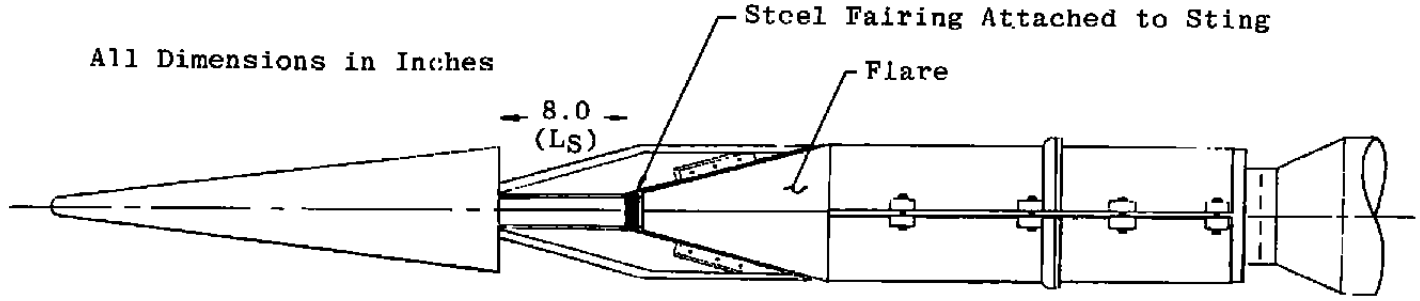

a. Plate 1 installed, $L_S/D = 1.0$

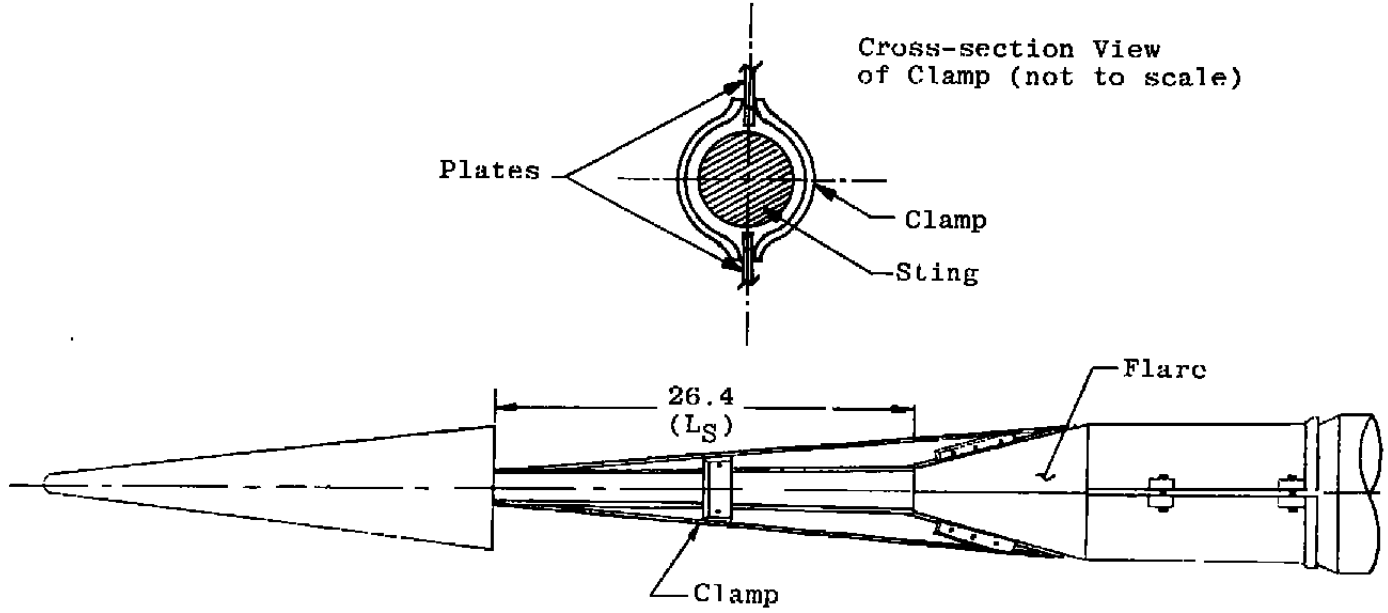

b. Plate 8 installed, $L_S/D = 3.3$

Figure 4. Details of splitter plate configurations.

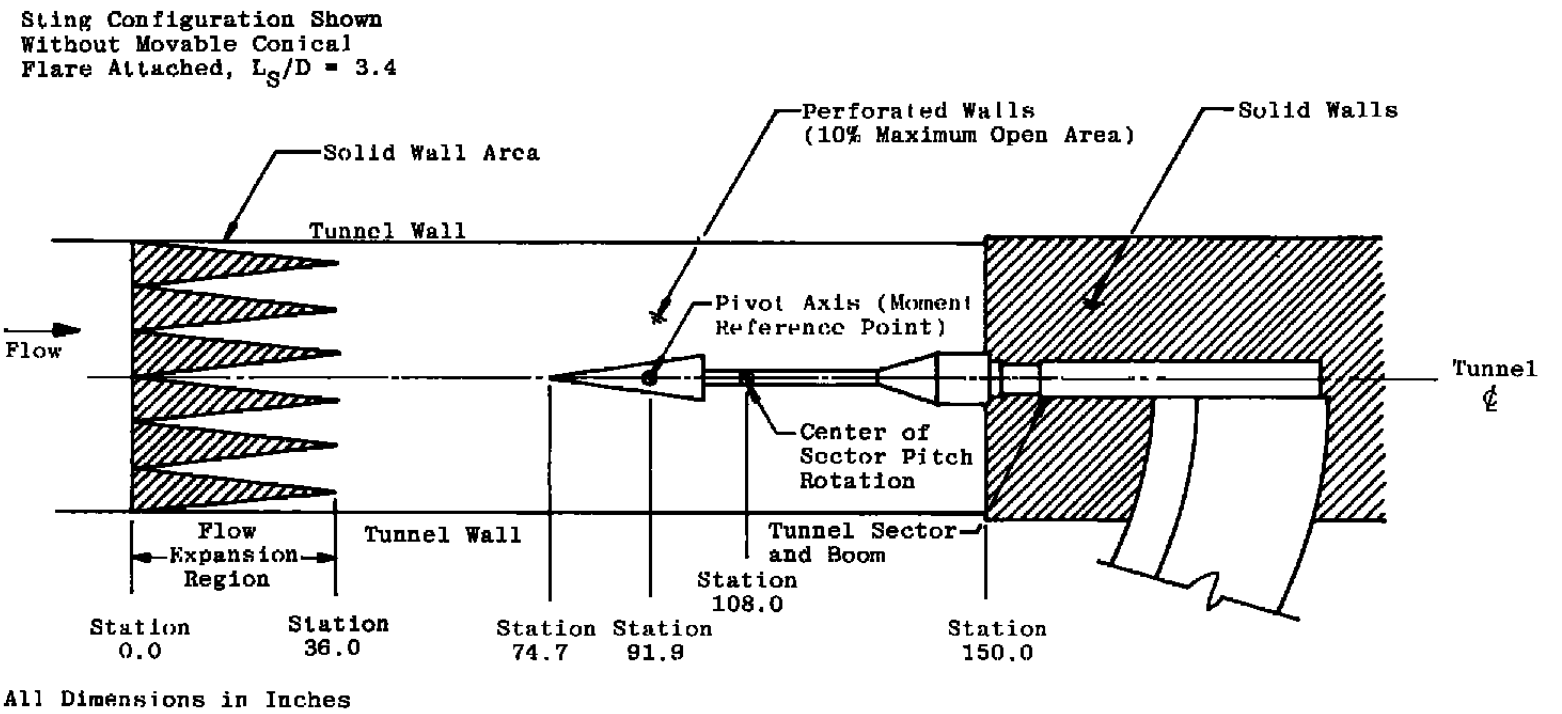

Figure 5. Sketch of model installation in aerodynamic wind tunnel (4T).

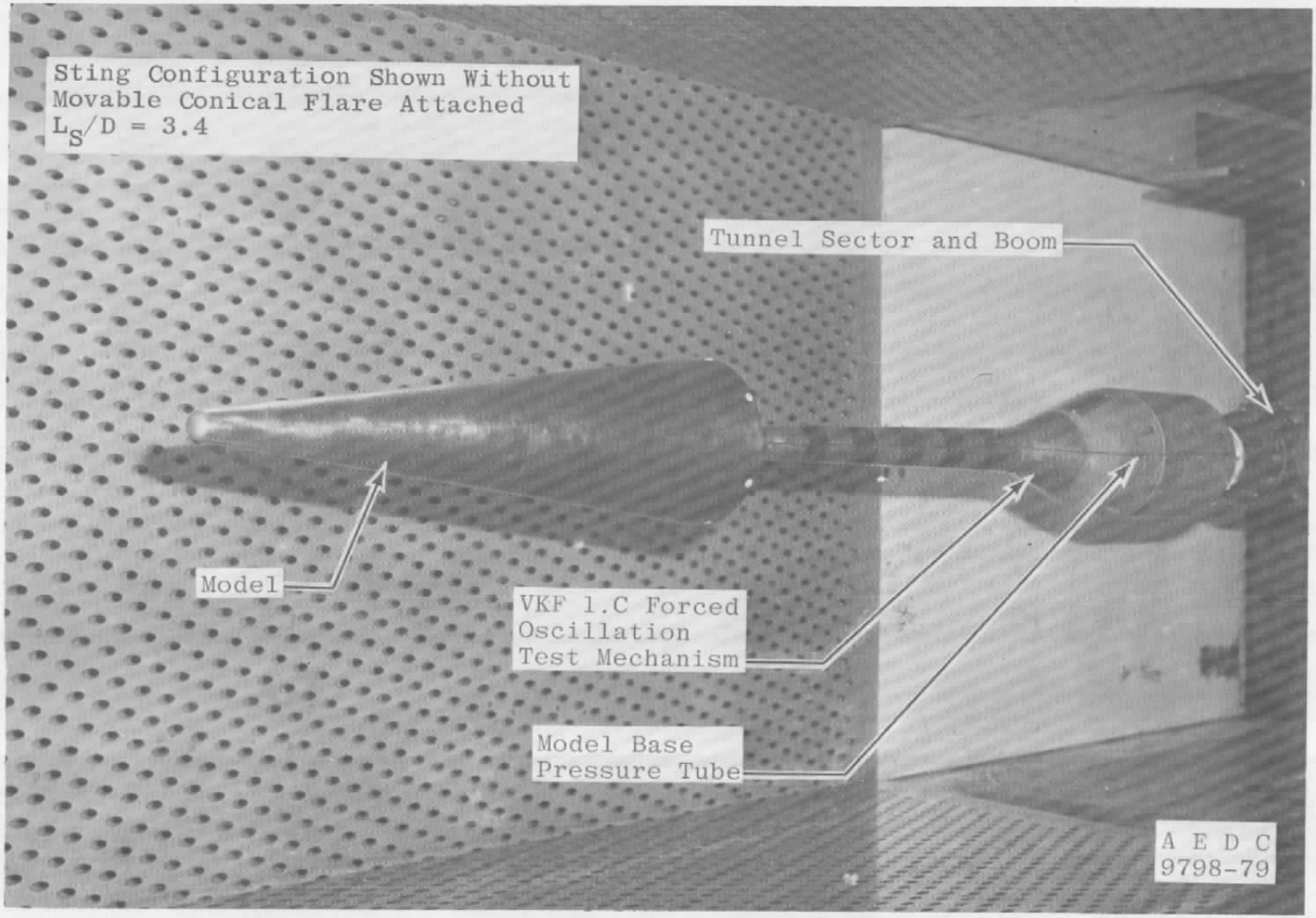

Figure 6. Photograph of model installation in aerodynamic wind tunnel (4T).

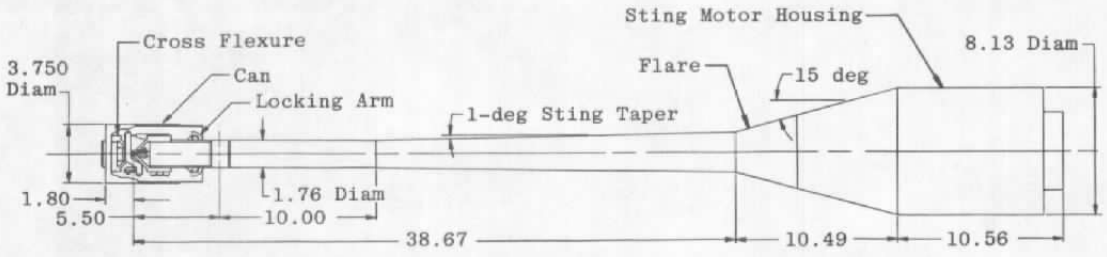

a. Details of test mechanism

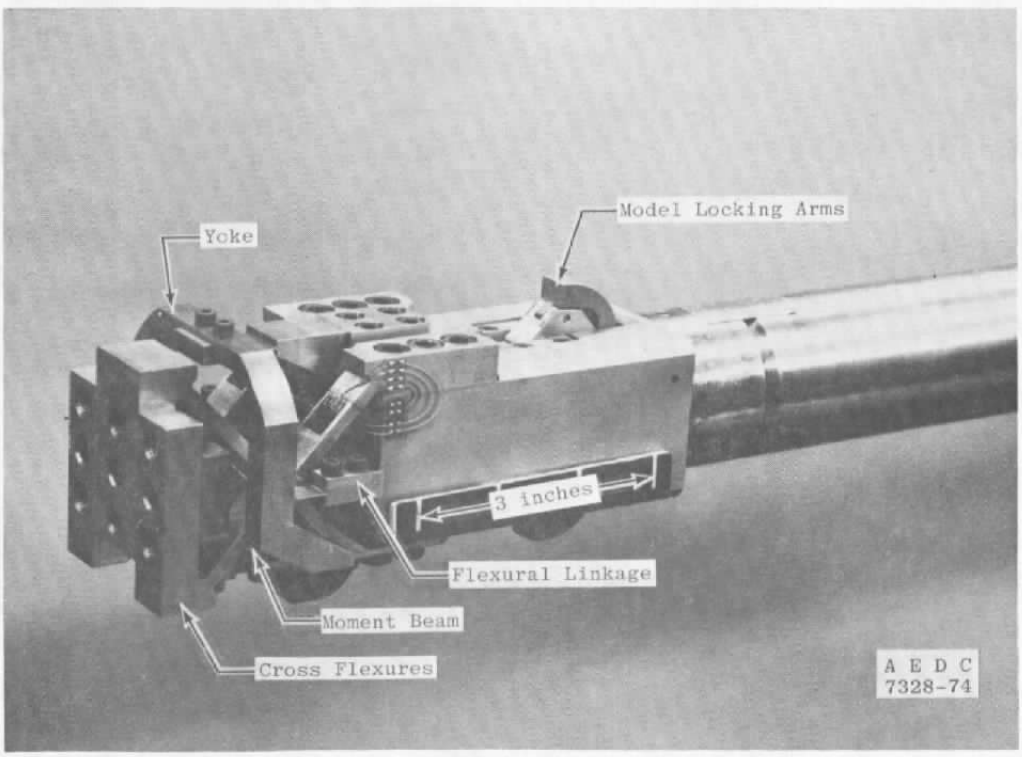

b. Photograph of cross flexure pivot

Figure 7. Details and photograph of VKF 1.C forced-oscillation test mechanism.

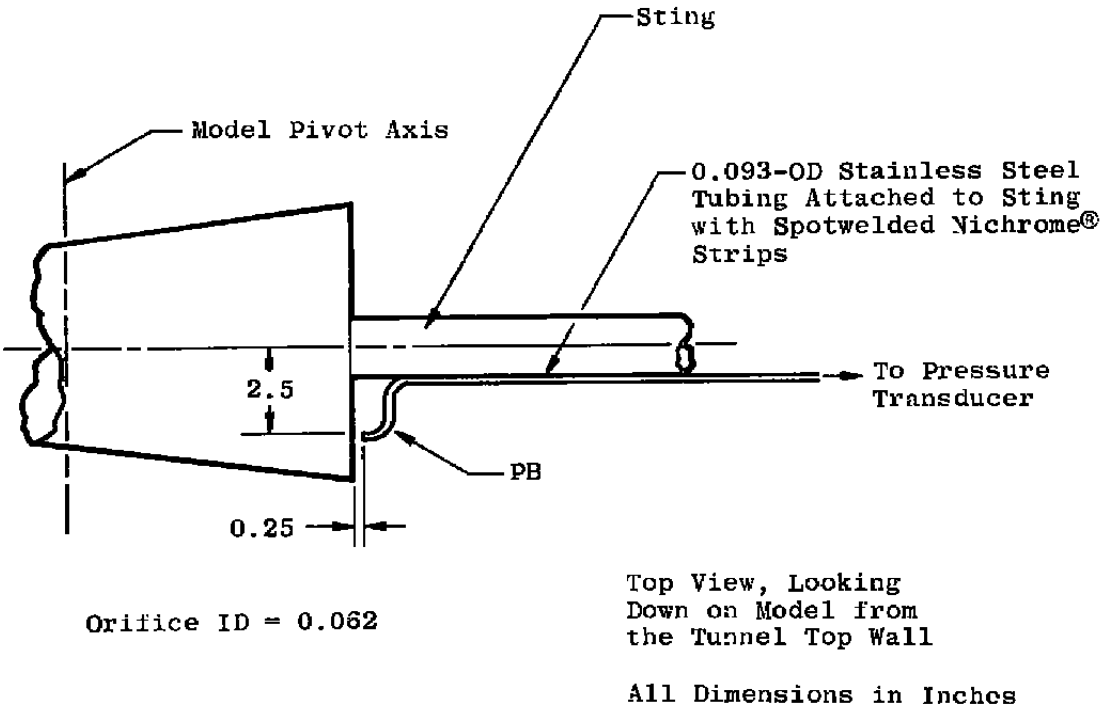

Figure 8. Location of base-pressure orifice.

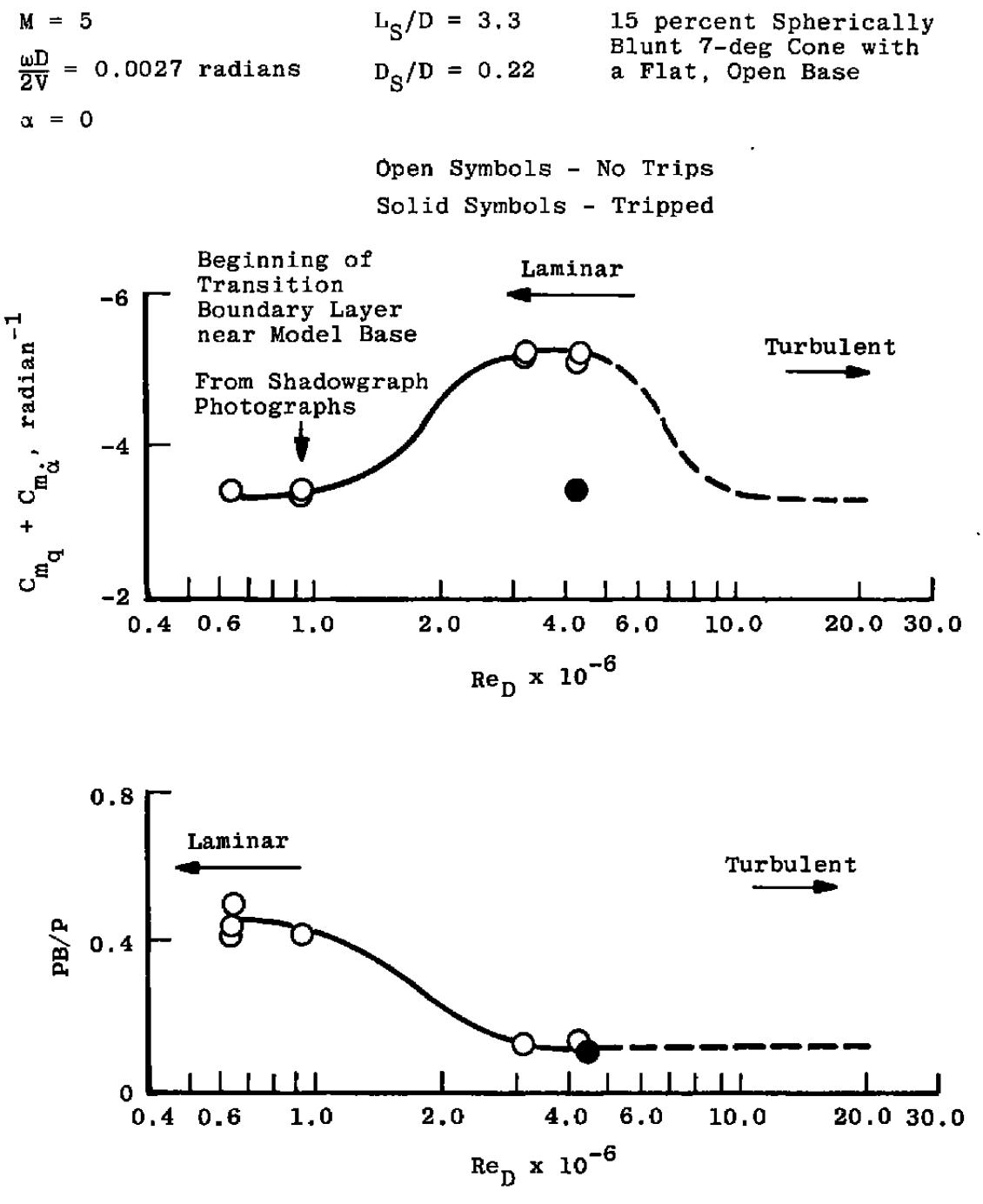

Figure 9. Typical trends of damping derivatives and base-pressure ratio as a function of Reynolds number and boundary-layer state (from Ref. 2).

Sym	Trip	M	$\frac{\omega D}{2V}$, radians
◐	None	0.2	0.048
◧	2	0.2	0.048
◑	None	0.95	0.011
▲	1	0.95	0.011
◨	2	0.95	0.011
○	None	1.3	0.008
△	1	1.3	0.008
□	2	1.3	0.008

$\alpha = 0$
$\theta = \pm 1$ deg
$L_S/D \geq 3.0$

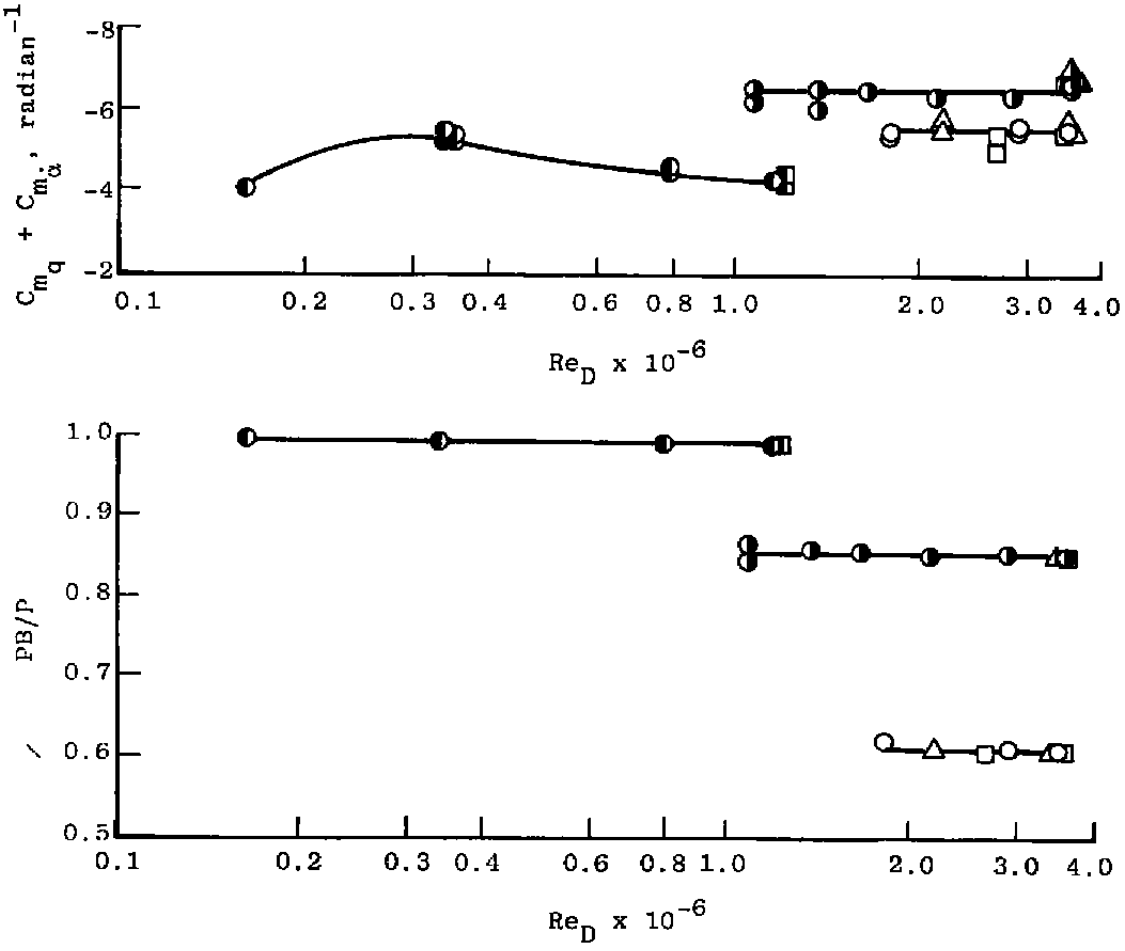

Figure 10. Variation of pitch-damping derivatives and base-pressure ratio as a function of Reynolds number at subsonic and transonic Mach numbers.

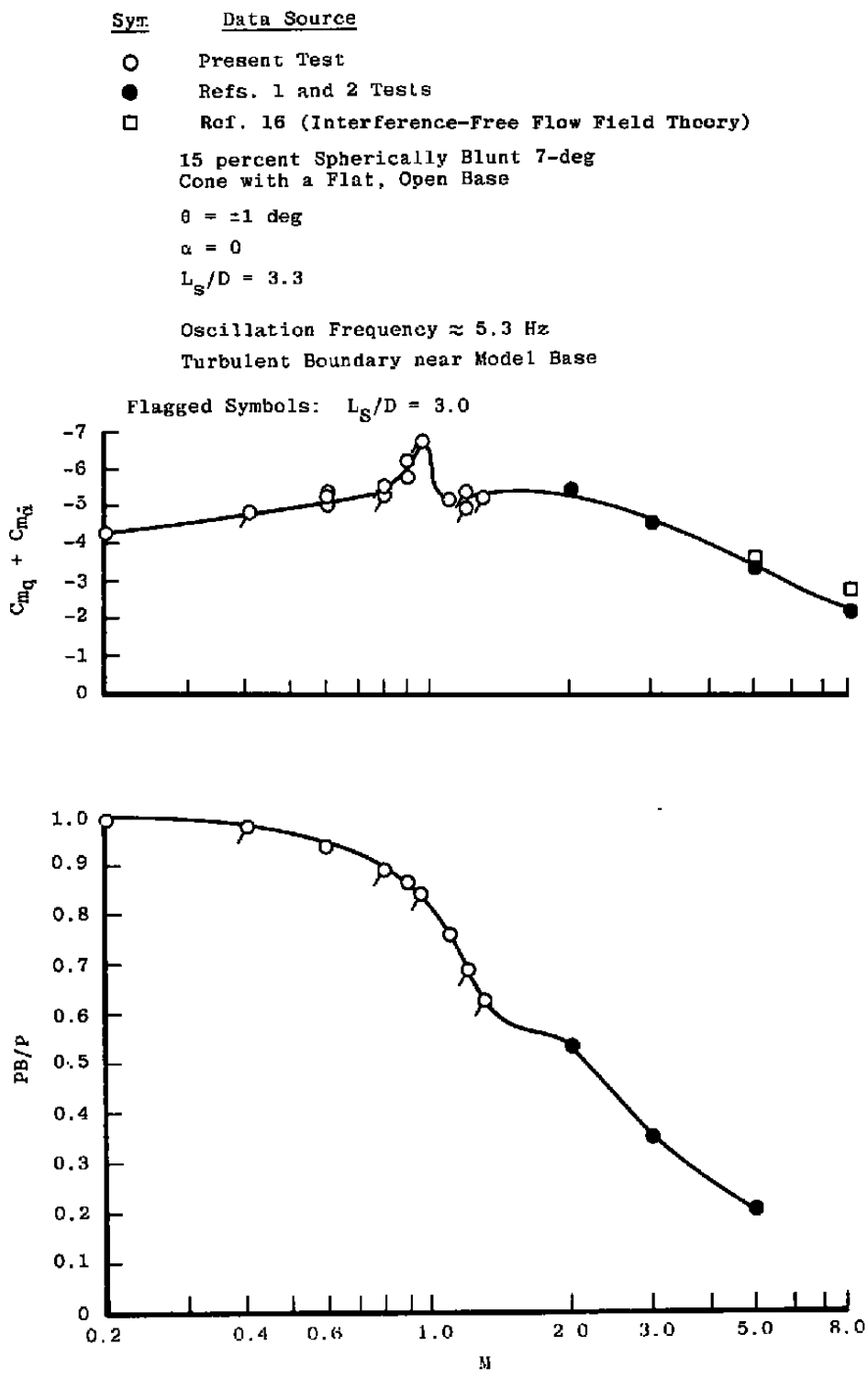

Figure 11. Variation of pitch-damping derivatives and base-pressure ratio over the subsonic-to-hypersonic range.

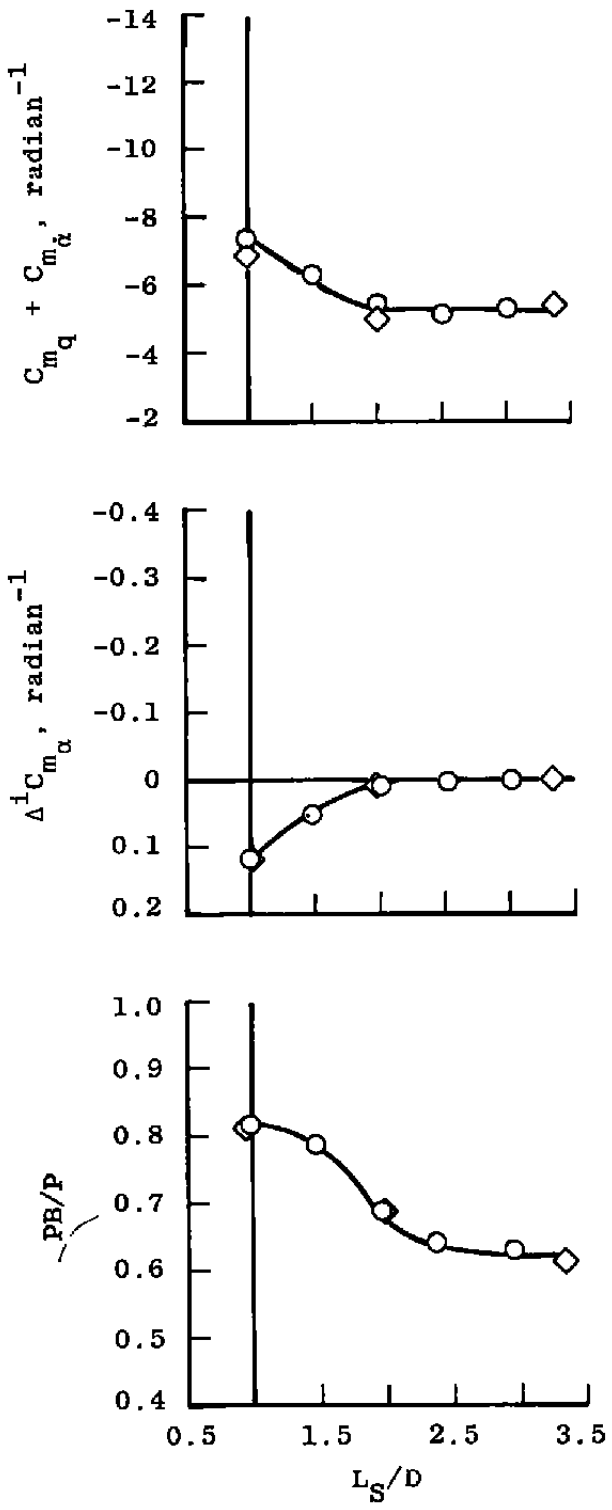

Sym	$Re_D \times 10^{-6}$
○	1.8
◇	3.3 and 3.5

$\frac{\omega D}{2V}$ = 0.008 radians

δ = ±1 deg

α = 0

D_S/D = 0.22

M = 1.3

15 percent Spherically Blunt 7-deg Cone with a Flat, Open Base

Figure 12. Effect of Reynolds number on data obtained with various effective sting lengths.

Sym	$\frac{\omega D}{2V}$, radians		
	0.006	M = 0.9 $Re_D = 1.7 \times 10^6$ $\theta = \pm 1$ deg	15 percent Spherically Blunt 7-deg Cone with a Flat, Open Base
	0.012		

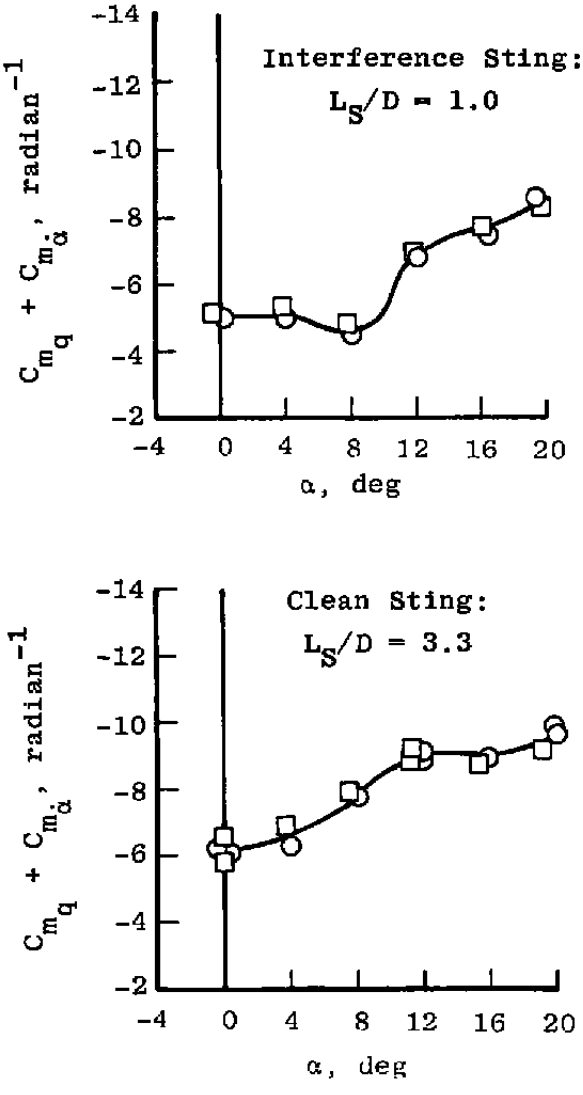

Figure 13. Effect of oscillation frequency on pitch-damping derivatives for interference and clean stings.

Sym	L_S/D
□	1.0
▽	1.5
△	2.0
◁	2.5
◇	3.0
○	3.3

$Re_D = 0.3 \times 10^6$

$\frac{\omega D}{2V} = 0.048$ radians

$\theta = \pm 1$ deg

$D_S/D = 0.22$

15 percent Spherically Blunt 7-deg Cone with a Flat, Open Base

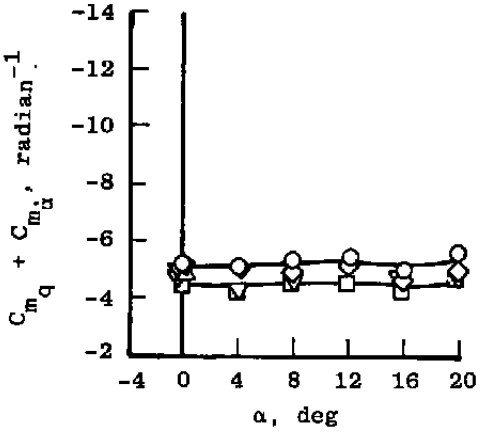

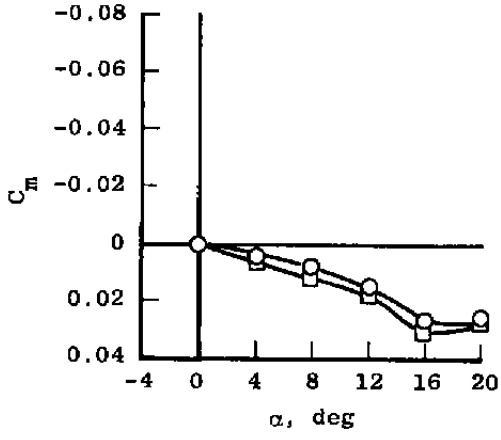

a. M = 0.2

Figure 14. Effect of angle of attack on sting-length interference.

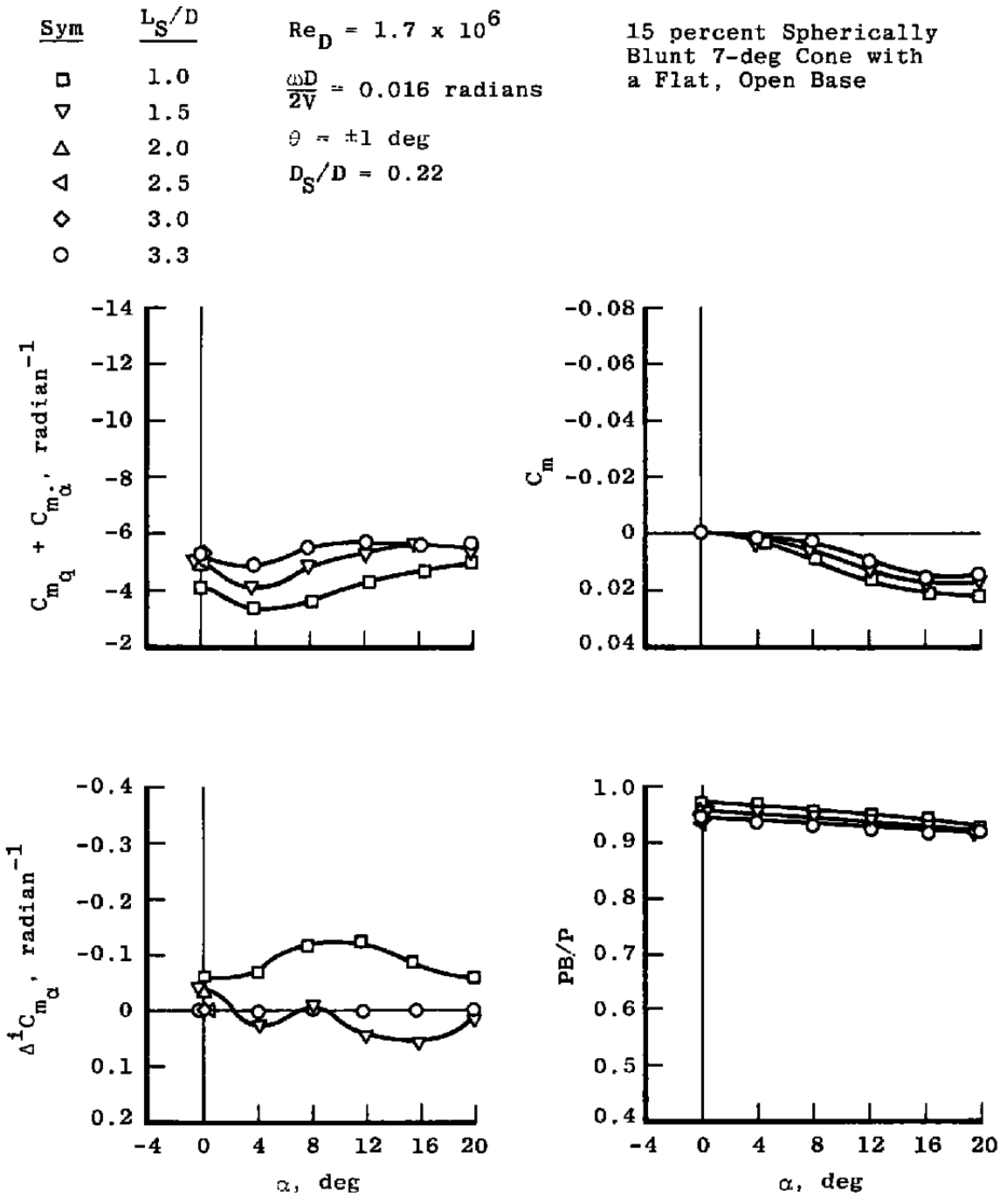

b. M = 0.6

Figure 14. Continued.

Sym	L_S/D
□	1.0
▽	1.5
△	2.0
◁	2.5
◇	3.0
○	3.3

$Re_D = 1.7 \times 10^6$

$\frac{\omega D}{2V} = 0.011$ radians

$\theta = \pm 1$ deg

$D_S/D = 0.22$

15 percent Spherically Blunt 7-deg Cone with a Flat, Open Base

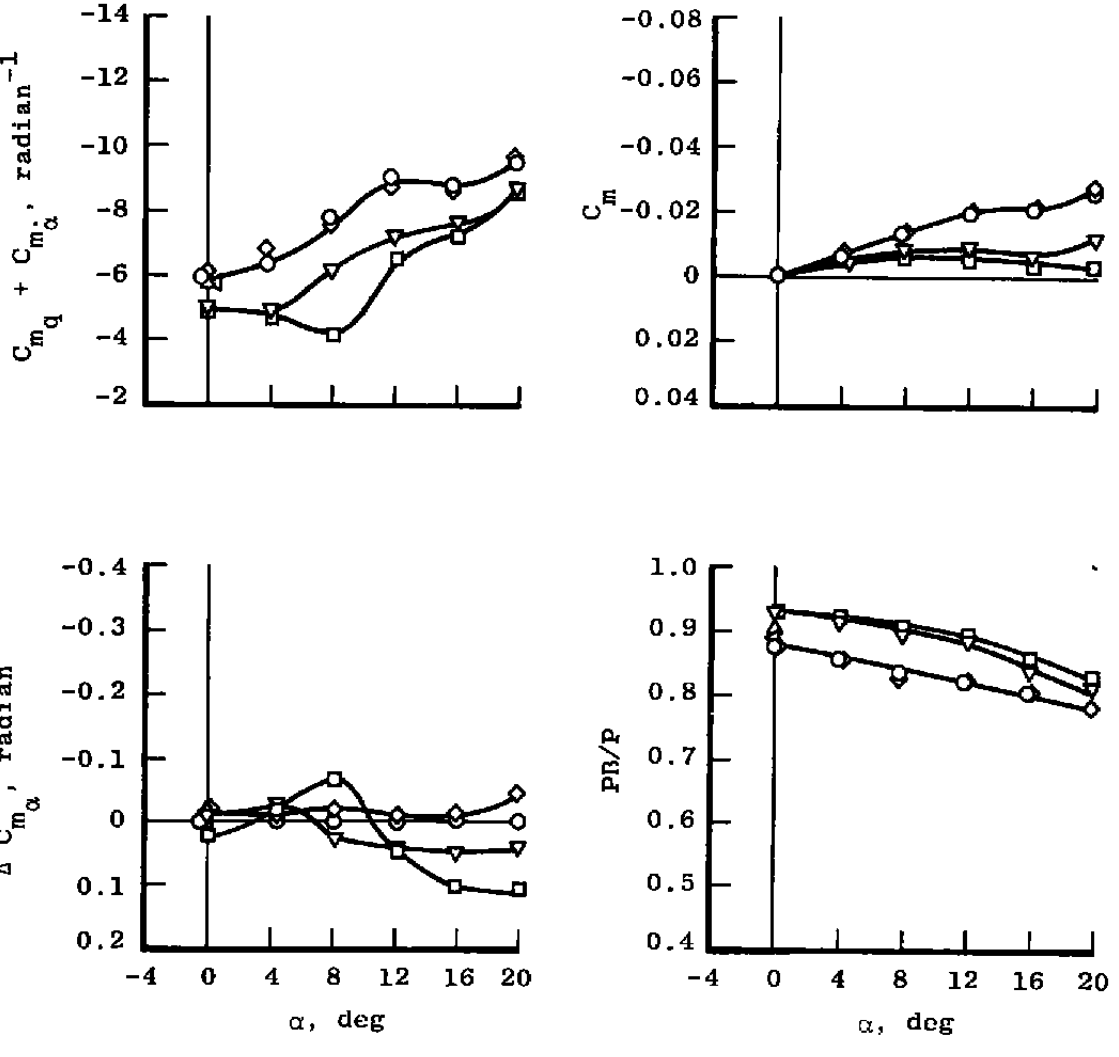

c. M = 0.9

Figure 14. Continued.

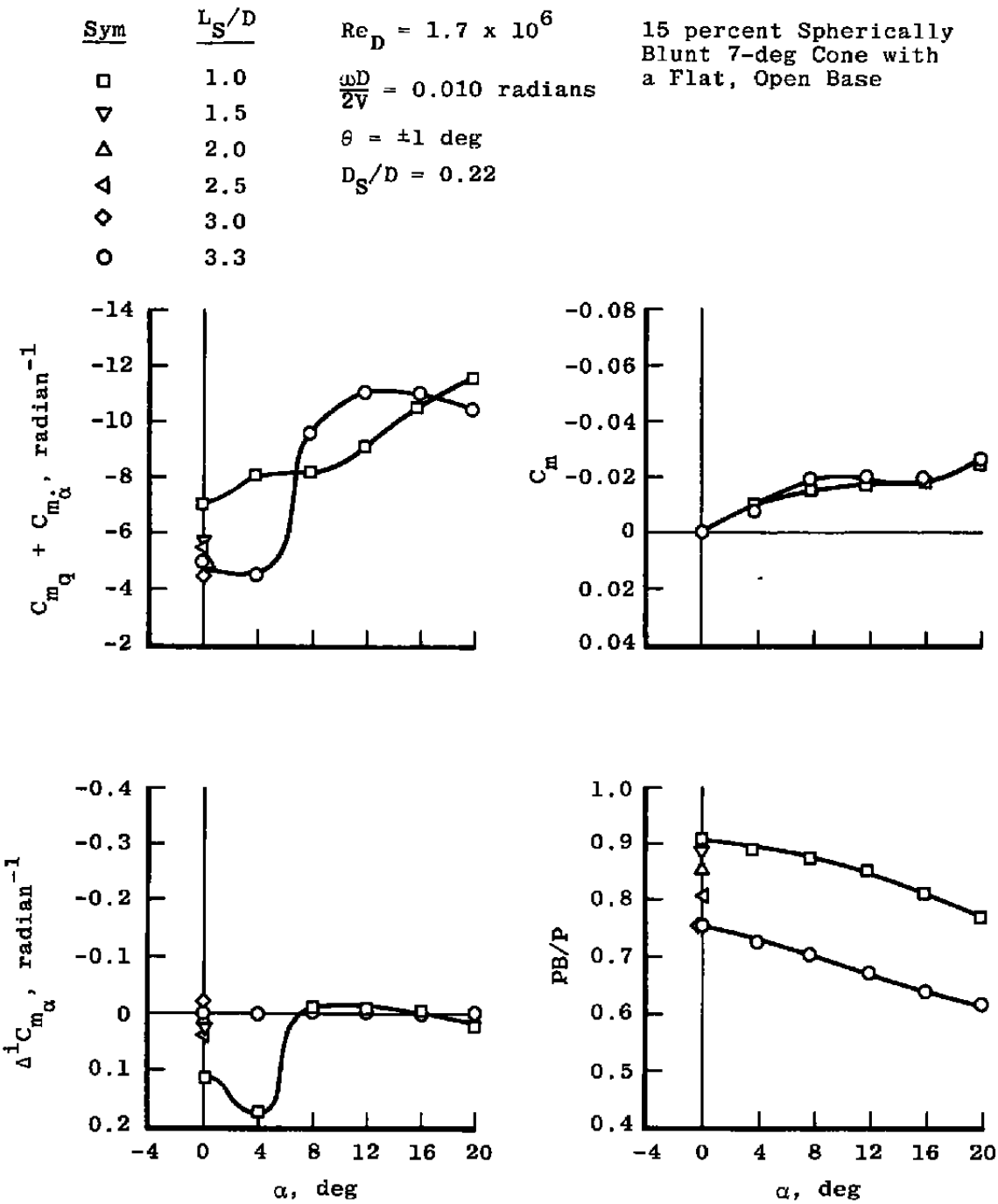

d. M = 1.10
Figure 14. Continued.

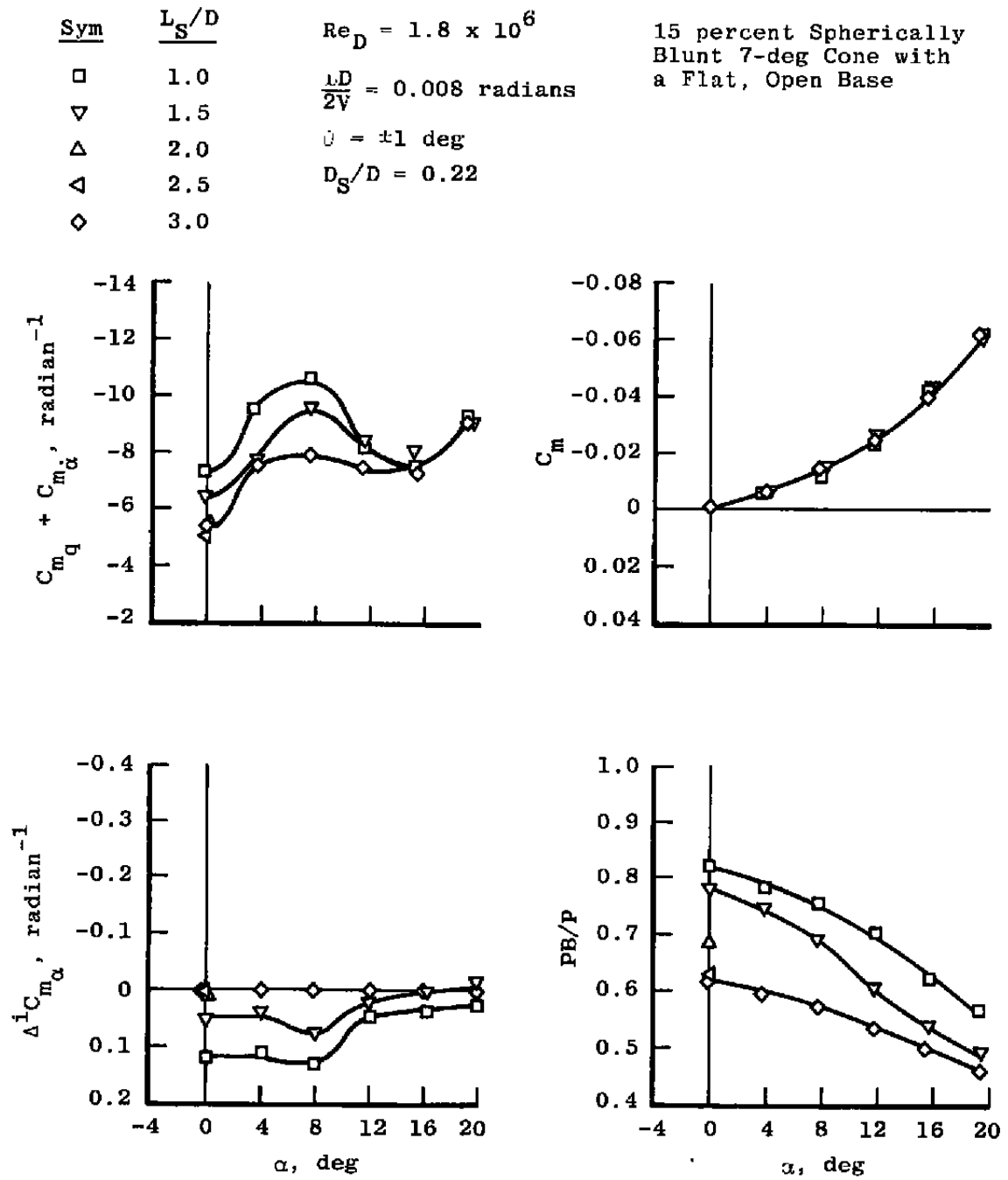

e. M = 1.30

Figure 14. Concluded.

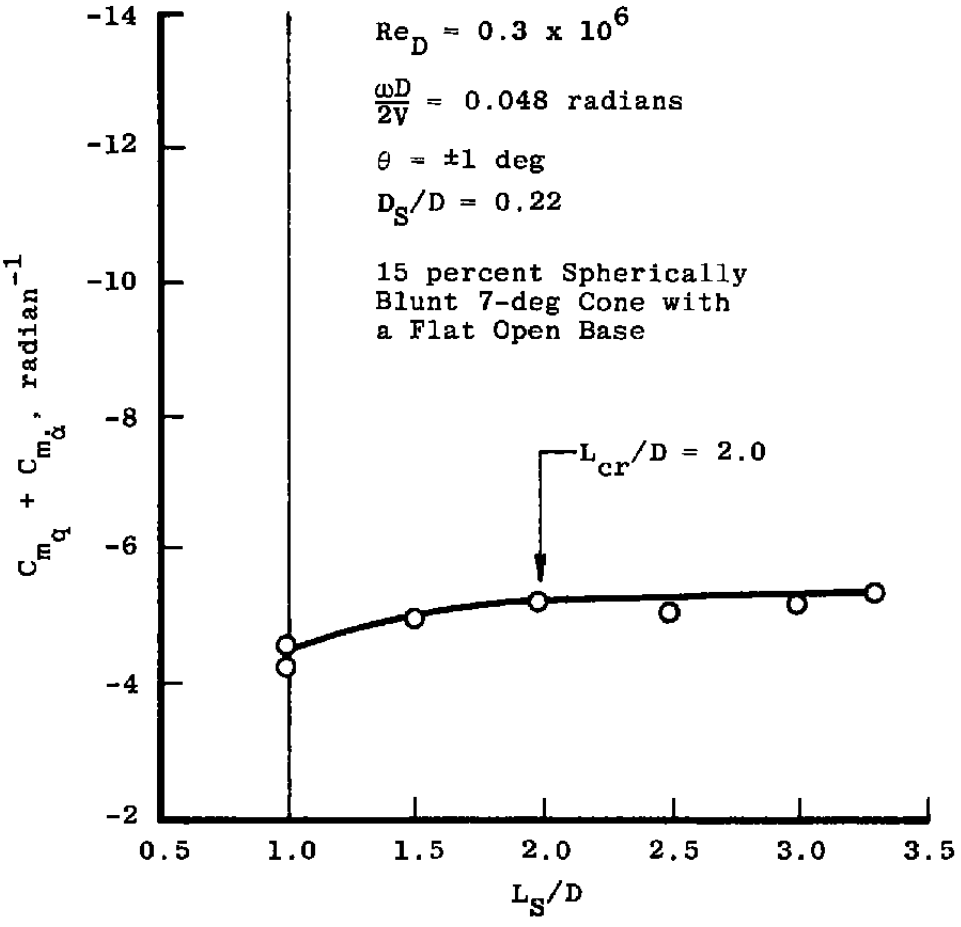

a. M = 0.2

Figure 15. Evaluation of critical sting length at $\alpha = 0$.

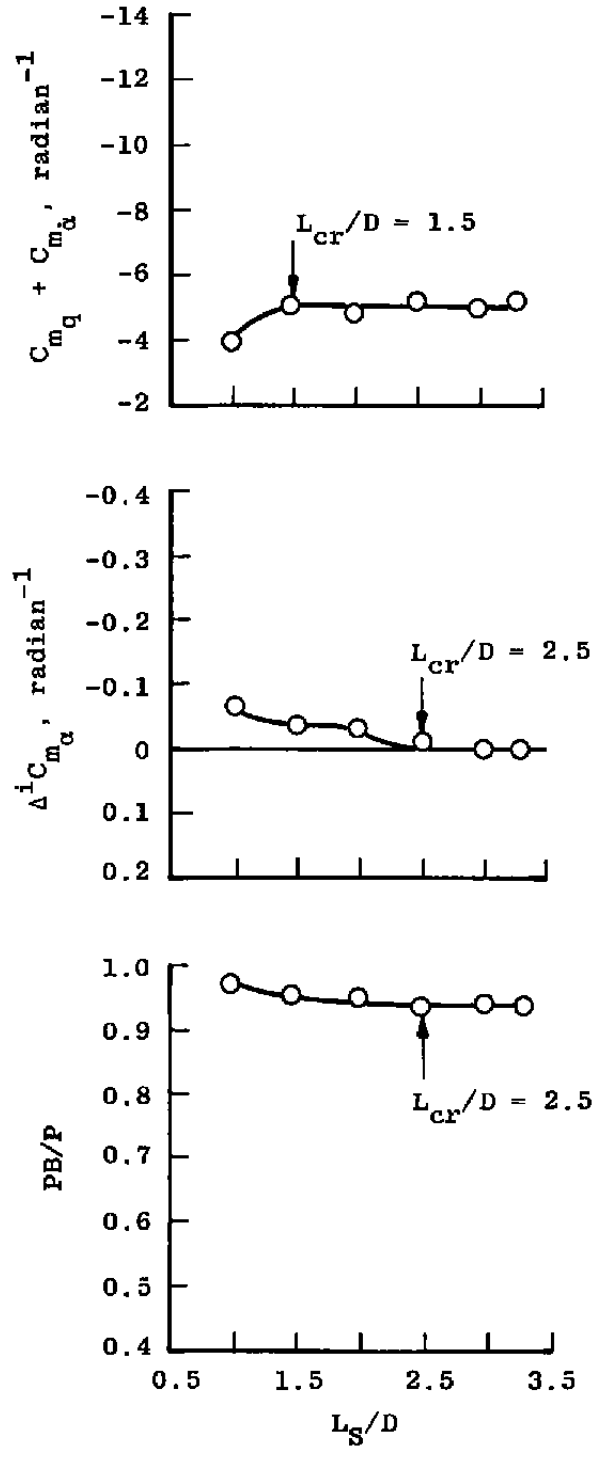

b. M = 0.6

Figure 15. Continued.

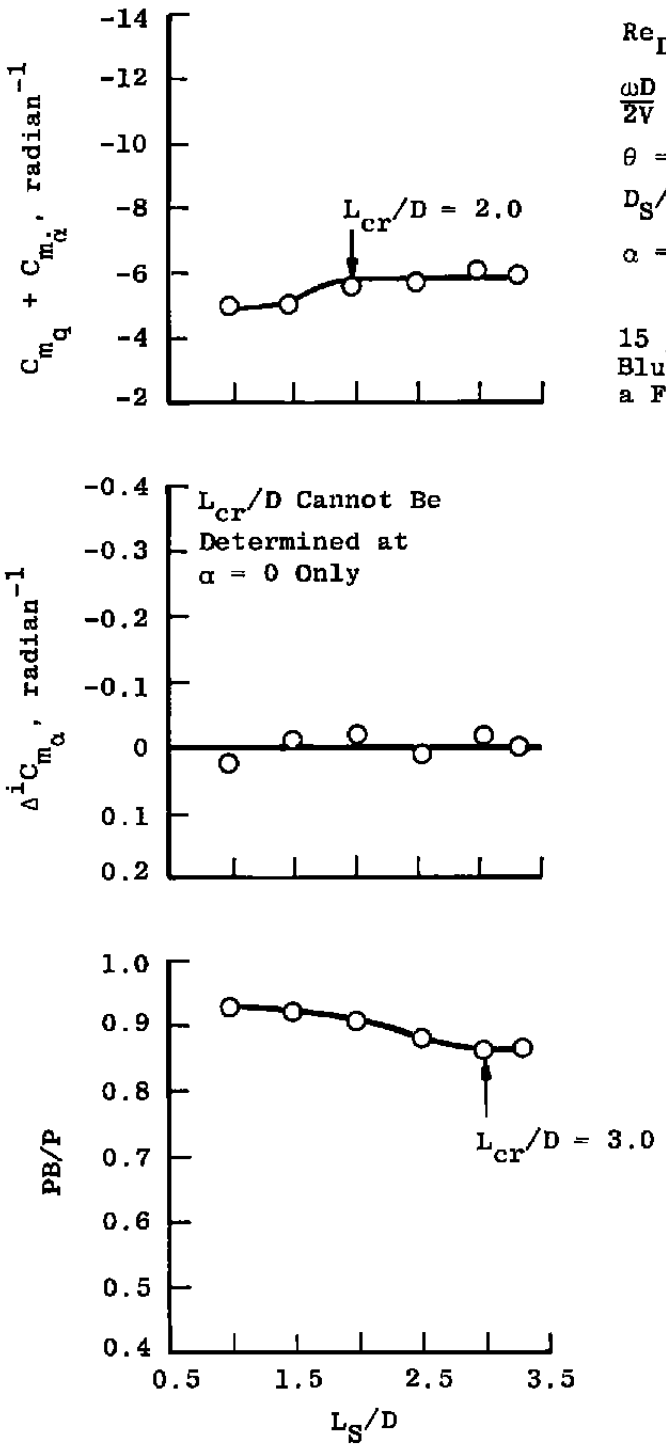

c. M = 0.9

Figure 15. Continued.

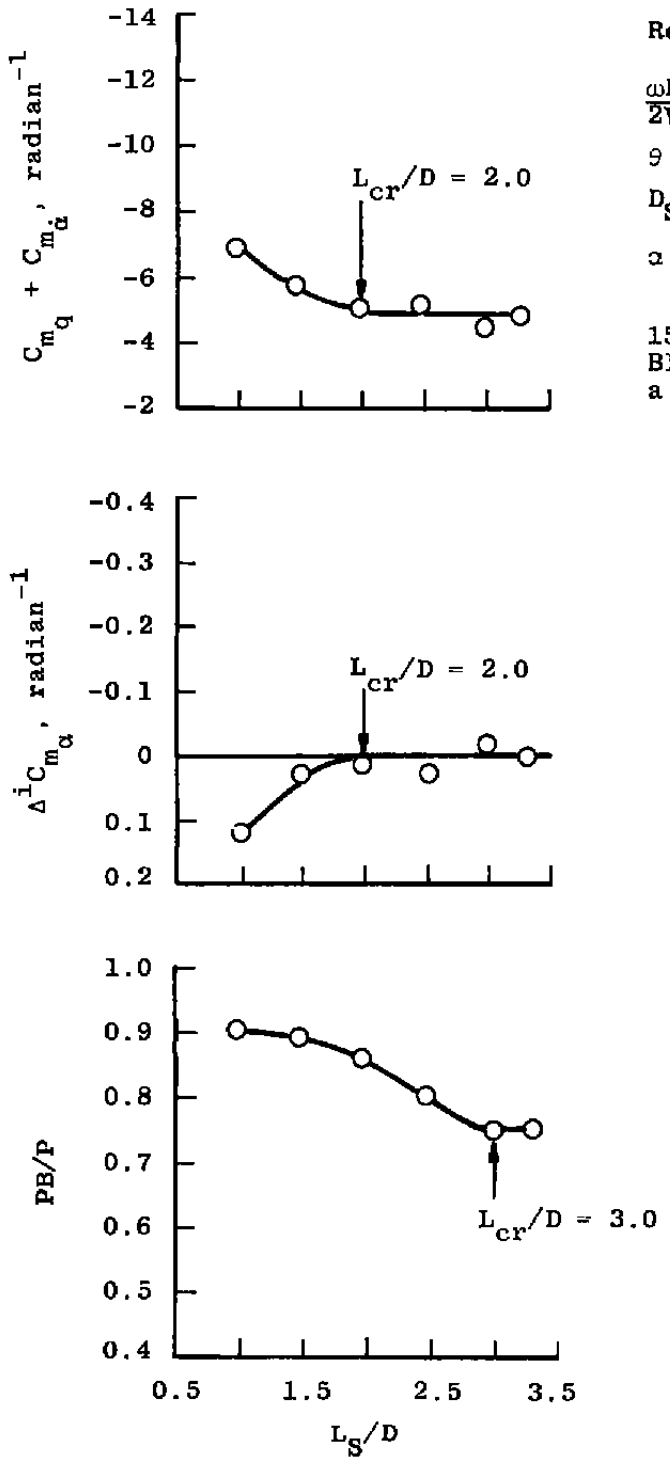

$Re_D = 1.7 \times 10^6$

$\frac{\omega D}{2V}$ = 0.010 radians

$\vartheta = \pm 1$ deg

$D_S/D = 0.22$

$\alpha = 0$

15 percent Spherically Blunt 7-deg Cone with a Flat, Open Base

d. M = 1.10

Figure 15. Continued.

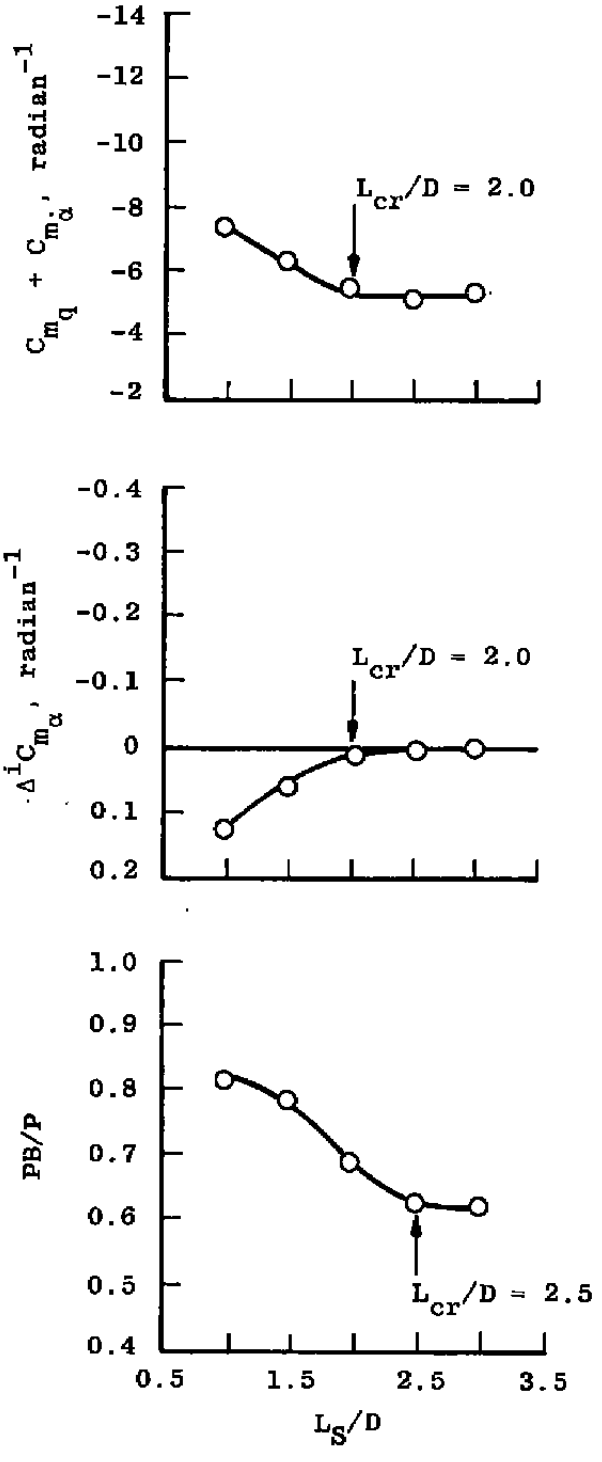

$Re_D = 1.8 \times 10^6$

$\frac{\omega D}{2V} = 0.008$ radians

$\delta = \pm 1$ deg

$D_S/D = 0.22$

$\alpha = 0$

15 percent Spherically Blunt 7-deg Cone with a Flat, Open Base

e. M = 1.3

Figure 15. Concluded.

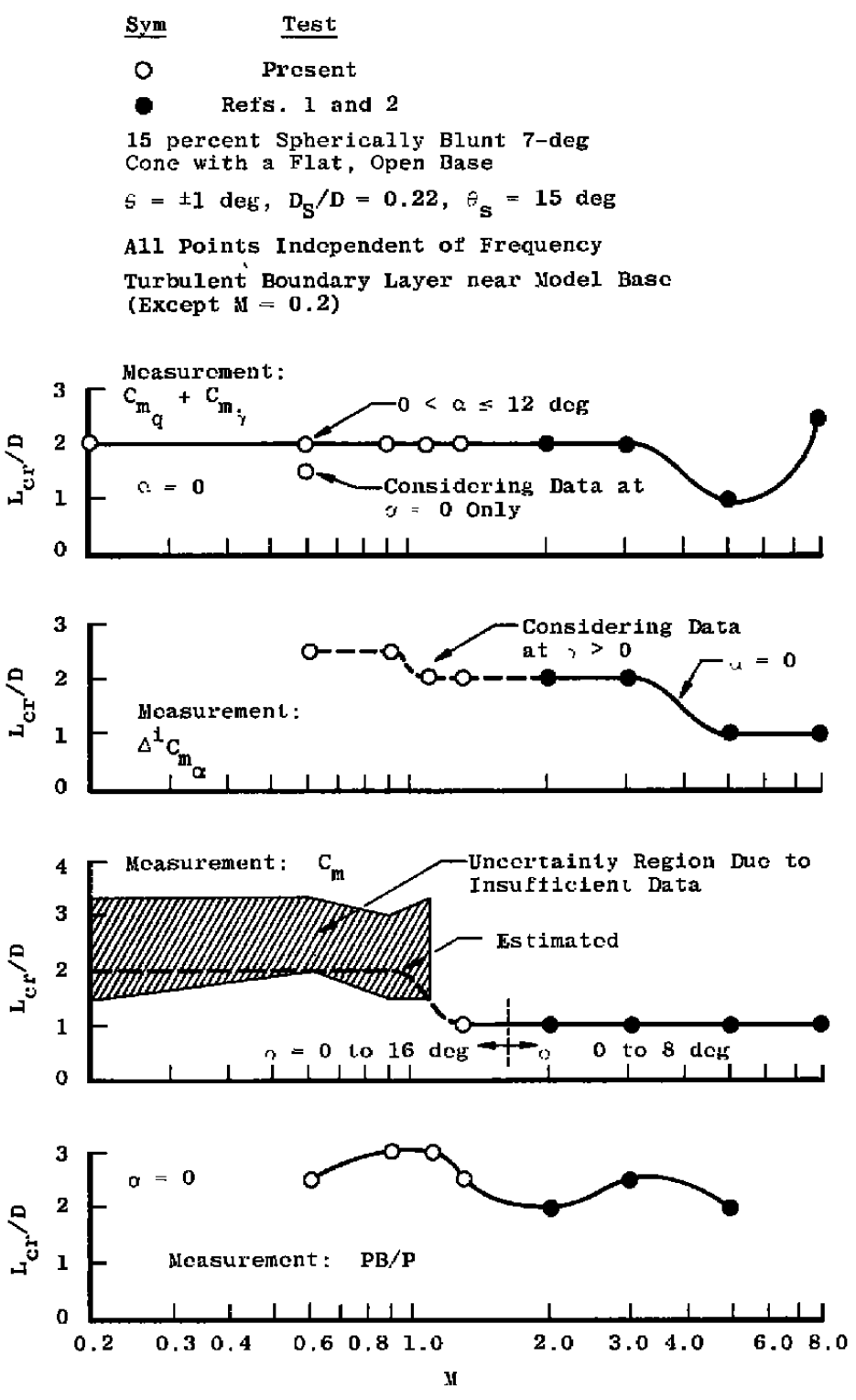

Figure 16. Variation of critical sting length with Mach number for various measurements.

Sym	θ_s, deg	D_S/D	Source	Model
◇	2.5	0.33	Ref. 15 Data	5-caliber Cone-Cylinder
– – – – –	4	0.50	Ref. 14 Data	10-caliber Ogive-Cylinder
□	5	0.33	Ref. 15 Data	5-caliber Cone-Cylinder
——	8	0.50	Ref. 14 Data	10-caliber Ogive-Cylinder
△	10	0.33	Ref. 15 Data	5-caliber Cone-Cylinder
·	12	0.50	Ref. 14 Data	10-caliber Ogive-Cylinder
○	15	0.22	Present and Ref. 2 Data	7-deg Cone, 15-percent Bluntness
◁	15	0.33	Ref. 15 Data	5-caliber Cone-Cylinder
◁	15	0.50	Ref. 13 Data	9.15-caliber Ogive-Cylinder
◇	20	0.33	Ref. 15 Data	5-caliber Cone-Cylinder

Note. All ogive- or cone-cylinder models had no boattail.

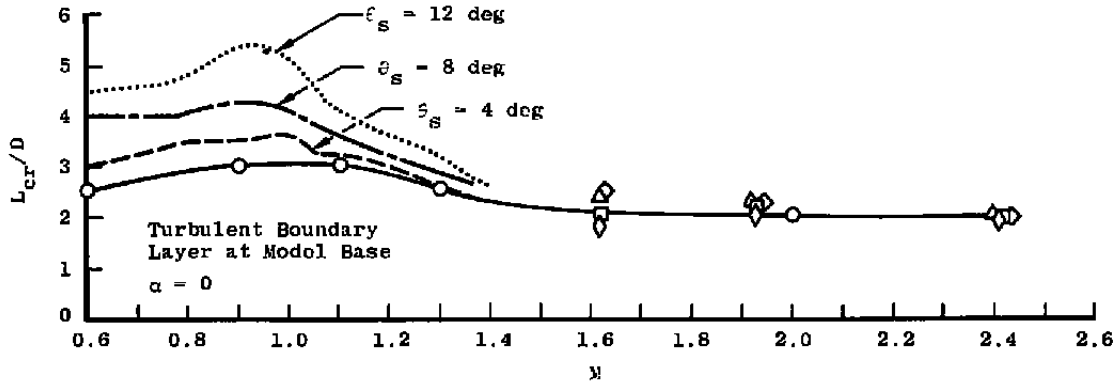

a. Effect of flare angle

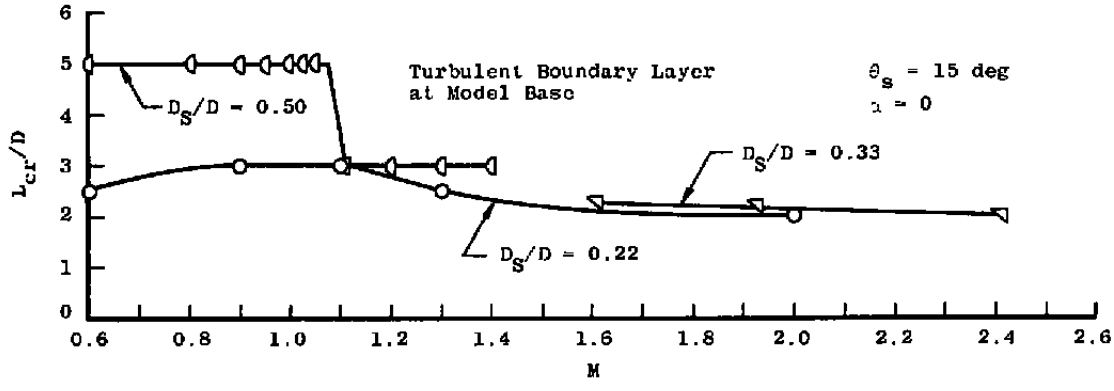

b. Effect of sting diameter

Figure 17. Comparison of critical sting length defined by base-pressure measurements.

Sym	Plate No.
○	None
△	1
◇	8

M = 0.9
$Re_D = 1.7 \times 10^6$

15 percent Spherically Blunt 7-deg Cone with a Flat, Open Base

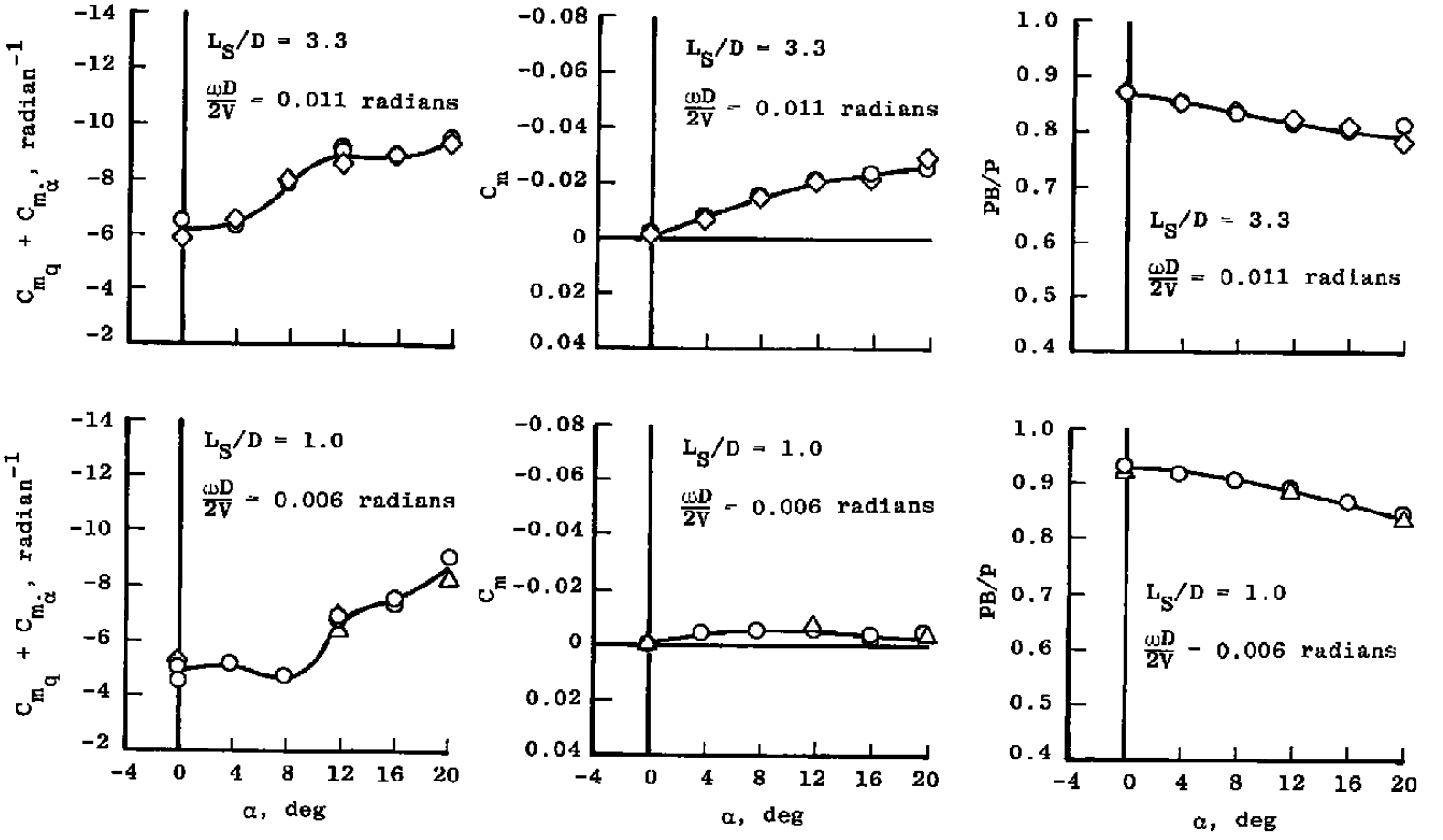

Figure 18. Effect of splitter plates.

Table 1. Test Conditions[a]

Test Condition	M	PT, psfa	TT, °R	Q, psf	P, psf	V, ft/sec	ωD/2V, radians Frequency = 5.3 Hz	ωD/2V, radians Frequency = 2.9 Hz	$Re_D \times 10^{-6}$
1	0.2	400	554	11	389	230	0.0483	---	0.16
2[b]	↓	820	550	22	797	230	0.0483	0.0264	0.33
3		2,000	566	54	1,945	232	0.0478	---	0.78
4		3,200	586	87	3,112	236	0.0470	---	1.20
5[c]		3,600	593	98	3,501	238	0.0466	0.0255	1.33
6	0.4	870	553	87	779	454	0.0244	---	0.67
7[c]	0.6	410	558	81	321	671	0.0165	---	0.43
8[c]	↓	1,300	549	257	1,019	666	0.0167	---	1.39
9[b]		1,630	569	322	1,278	678	0.0164	0.0090	1.66
10[c]		3,200	581	632	2,508	685	0.0162	0.0089	3.18
11	0.8	1,320	555	388	866	870	0.0128	---	1.66
12[b]	0.9	1,260	556	422	745	965	0.0115	0.0063	1.66
13[c]	0.9	2,800	603	939	1,656	1,005	0.0110	---	3.33
14	0.95	800	550	283	448	1,005	0.0110	---	1.09
15	↓	1,020	554	360	571	1,009	0.0110	---	1.38
16		1,220	556	431	683	1,011	0.0110	---	1.64
17		1,600	560	565	895	1,014	0.0109	---	2.13
18		2,200	567	778	1,231	1,021	0.0109	---	2.88
19		2,800	578	990	1,567	1,030	0.0108	---	3.58
20[b]	1.10	1,200	555	476	562	1,140	0.0097	---	1.67
21[c]	1.10	2,640	600	1,047	1,236	1,185	0.0094	---	3.33
22	1.20	1,200	556	499	495	1,222	0.0091	---	1.68
23[b]	1.30	1,300	556	555	469	1,299	0.0085	---	1.82
24	↓	1,600	568	683	577	1,313	0.0085	---	2.17
25		2,200	578	939	794	1,325	0.0084	---	2.92
26		2,560	588	1,093	924	1,336	0.0083	---	3.33
27		2,700	591	1,153	974	1,339	0.0083	---	3.48

Notes:

[a] Angle-of-attack range shown in Table 2

[b] Primary test conditions

[c] Data not presented in this report, but presented in Ref. 3

Table 2. Test Summary Log

Frequency, Hz	L_S/D	Trip No.[a]	Plate No.[b]	Test Conditions[c]	α, deg
2.9	3.3	None	None	2, 9, 12	0 to 20
↓	3.0	↓	↓	2, 9, 12	0
↓	2.5	↓	↓	2, 9, 12	0
↓	2.0	↓	↓	2, 9[d], 12[d]	0 to 20
↓	1.5	↓	↓	2, 9, 12	0
↓	1.0	↓	↓	2, 5[d], 9, 10[d], 12	0 to 20
↓	1.0	↓	1	2, 9[e], 12[e]	0 to 20
5.3	3.4	↓	None	1, 3, 4, 7, 8[f], 10[g], 14, 15[h],	0
↓	↓	↓	↓	17, 18, 19, 23, 25, 27,	↓
↓	↓	1	↓	19, 24, 27,	↓
↓	↓	2	↓	4, 19, 25, 27,	↓
↓	3.3	None	↓	2, 9, 12, 20	0 to 20
↓	3.0	↓	↓	2[d], 6[d], 9[d], 11, 12,	↓
↓	3.0	↓	↓	15[h], 16, 20[d], 22[d], 23	↓
↓	2.5	↓	↓	2, 9, 12, 20, 23	0
↓	2.0	↓	↓	2, 5, 9, 10, 12,	↓
↓	2.0	↓	↓	13, 20, 21, 23, 26	↓
↓	1.5	↓	↓	2, 5, 9[d], 12[d], 20[d], 21[d], 23	0 to 20
↓	1.0	↓	↓	2, 5[d], 6[d], 9, 10[d], 11[d], 12,	↓
↓	1.0	↓	↓	13[d], 20, 21[d], 22[d], 23, 26[d]	↓
↓	3.3	↓	8	2, 9, 12	↓

$\delta = \pm 1$ deg $\omega D/2V = 0.006 \rightarrow 0.049$

Notes:

[a] As shown in Fig. 1

[b] As shown in Figs. 3 and 4

[c] As listed in Table 1

[d] Data obtained at α = 0 only

[e] Data obtained at α = 0, 12, 20 deg only

[f] Data obtained at α = 0, 15, 26 deg only

[g] Data obtained at α = 0, 25 deg only

[h] Data obtained at α = 0 to 24 deg

Table 3. Estimated Uncertainties
a. Basic Steady-State Measurements

Parameter Designation	STEADY-STATE ESTIMATED MEASUREMENT*							Range	Type of Measuring Device	Type of Recording Device	Method of System Calibration
	Precision Index (S)			Bias (B)		Uncertainty ±(B + t95S)					
	Percent of Reading	Unit of Measurement	Degree of Freedom	Percent of Reading	Unit of Measurement	Percent of Reading	Unit of Measurement				
PT, psfa	±(0.04% + 0.15)		30	±(0.11% + 1)		±(0.2% + 1.3)		0 to 1,500	Datametrics Barocel Model 538AX-93 0-4000 psfa	Datametrics Electronic Manometer C-1018	In-Place Calibration with a Precision Pressure Standard
		±0.7	30		±2.9		14.3	1,500 to 4,000			
TT, °R	—	±0.1	6	—	±0.55	—	±0.77	410 to 610	Dual Chromel®-Alumel® Thermocouples	Newport Model 2600KF Digital Thermometer	Voltage Standard Substitution using a Stirred Ice Bath Thermocouple Reference
PS, psfa	—	±1.0	32	±(0.14% + 1)		±(0.14% + 3)		0 to 2,160	Sunstrand (Kistler) 314D Servo Pressure Transducer	Preston Amplifier used with a Preston G-MAD-3 for A/D Conversion	In-Place Calibration with a Precision Pressure Standard
Support System Sector and Boom Angle, deg	±(0.014% + 0.004)		7	—	±0.029	±(0.03% + 0.038)		-7.5 to 78	Clifton Precision Products Model CG-10-AS-1 Synchro Transmitter	Theta Model C-5280 Digital Indicator	In-Place Calibration by Comparison to an Inclinometer
Frequency, Hz	0.0025	—	2	—	0	0.01	—	0 to 10	A/D Frequency Convertor Built by VKF	Digital Data Acquisition System (DDAS)	Compared with a Frequency Standard
Model Angular Displacement about the Pivot Axis, deg											
a. 0.10 in. thick cross flexures	—	0.024	26	—		—	0.048	±3	Bonded Strain Gages		Static Loading
b. 0.15 in. thick cross flexures	—	0.017	32	—		—	0.034	±3			
Sting Angular Displacement, deg	—	0.008	32	—		—	0.014	±1			

*Thompson, J. W. and Abernethy, R. B. et al "Handbook Uncertainty in Gas Turbine Measurements" AEDC-TR-73-5 (AD 755356), February 1973.

Table 3. Continued
b. Basic Dynamic Measurements

Parameter Designation	STEADY-STATE ESTIMATED MEASUREMENT* Precision Index (S)			Bias (B)		Uncertainty ±(B + t95S)		Range	Type of Measuring Device	Type of Recording Device	Method of System Calibration
	Percent of Reading	Unit of Measurement	Degree of Freedom	Percent of Reading	Unit of Measurement	Percent of Reading	Unit of Measurement				
Out-of-Phase Torque, ft-lb	---	0.0001	10	0		---	0.0002	0 to 0.82	Bonded Strain Gages	Digital Data Acquisition System (DDAS)	In-place Moment Loading
In-Phase Torque, ft-lb	---	5.2×10^{-5}	10			---	0.0001	0 to 0.82			
In Phase Sting Moment, ft-lb	---	0.35	32			---	0.70	0 to 50			Static Loading
θ deg a. 0.10 in. thick cross flexures	---	0.024	26			---	0.048	±3			
b. 0.15 in. thick cross flexures	---	0.017	32			---	0.034	±3			

*Thompson, J. W., and Abernethy, R. B. et al. "Handbook Uncertainty in Gas Turbine Measurements." AEDC-TR-73-5 (AD 755356), February 1973

Table 3. Continued
c. Calculated Parameters

Parameter Designation	STEADY-STATE ESTIMATED MEASUREMENT*							Parameter Range	Test Conditions	
	Precision Index (S)			Bias (B)		Uncertainty ±(B + t95S)				
	Percent of Reading	Unit of Measurement	Degree of Freedom	Percent of Reading	Unit of Measurement	Percent of Reading	Unit of Measurement		M	Re_D x 10^{-6}
V, ft/sec	---	3.5		---	13.6	---	20.6	230	0.2	0.3
	---	0.9		---	3.5	---	5.3	678	0.6	1.7
	---	0.7		---	2.7	---	4.1	695	0.9	1.7
	---	0.6		---	2.4	---	3.6	1,140	1.1	1.7
	---	0.5		---	2.2	---	3.2	1,300	1.3	1.8
	---	0.4		---	1.5	---	2.3	1,336	1.3	3.3
Re_D x 10^{-6}	---	0.005		---	0.020	---	0.030	0.3	0.2	---
	---	0.002		---	0.010	---	0.014	1.7	0.6	---
	---	0.001		---	0.006	---	0.008	1.7	0.9	---
	---	0.001		---	0.006	---	0.007	1.7	1.1	---
	---	0.001		---	0.005	---	0.006	1.8	1.3	---
	---	0.001		---	0.007	---	0.008	3.3	1.3	---
Q, psf	---	0.66		---	2.6	---	3.9	22	0.2	0.3
	---	0.81		---	3.1	---	4.7	322	0.6	1.7
	---	0.53		---	1.9	---	3.0	422	0.9	1.7
	---	0.40		---	1.5	---	2.3	476	1.1	1.7
	---	0.33		---	1.2	---	1.8	555	1.3	1.8
	---	0.35		---	1.4	---	2.1	1,093	1.3	3.3

*Abernethy, R. B. et al. and Thompson, J. W. "Handbook Uncertainty in Gas Turbine Measurements," AEDC-TR-73-5 (AD 755356), February 1973.

Table 3. Continued
c. Continued

Parameter Designation	STEADY-STATE ESTIMATED MEASUREMENT*							Parameter Range	Test Conditions	
	Precision Index (S)			Bias (B)		Uncertainty ±(B + t_{95}S)				
	Percent of Reading	Unit of Measurement	Degree of Freedom	Percent of Reading	Unit of Measurement	Percent of Reading	Unit of Measurement		M	Re_D x 10^{-6}
P, psf	——	0.43		——	2.02	——	2.88	797	0.2	0.3
	——	0.72		——	2.30	——	3.74	1,278	0.6	1.7
	——	0.43		——	1.87	——	2.73	745	0.9	1.7
	——	0.43		——	1.58	——	2.44	562	1.1	1.7
	——	0.43		——	1.44	——	2.30	469	1.3	1.8
	——	0.58		——	2.02	——	3.18	924	1.3	3.3
M	——	0.003		——	0.012	——	0.018	0.2	——	0.3
	——	0.001		——	0.004	——	0.005	0.6	——	1.7
	——	0.001		——	0.003	——	0.004	0.9	——	1.7
	——	0.001		——	0.003	——	0.004	1.1	——	1.7
	——	0.001		——	0.003	——	0.004	1.3	——	1.8
	——	0.001		——	0.002	——	0.003	1.3	——	3.3
α, deg	——	0.030		——	0.040	——	0.100	0—28	——	

*Abernethy, R. B. et al. and Thompson, J. W. "Handbook Uncertainty in Gas Turbine Measurements." AEDC-TR-73-5 (AD 755356), February 1973.

Table 3. Concluded
c. Concluded

Parameter Designation	STEADY-STATE ESTIMATED MEASUREMENT*							Parameter Range	Test Conditions			
	Precision Index (S)			Bias (B)		Uncertainty ±(B + t_{95}S)						
	Percent of Reading	Unit of Measurement	Degrees of Freedom	Percent of Reading	Unit of Measurement	Percent of Reading	Unit of Measurement		M	$Re_D \times 10^{-6}$	α, deg	ωD/2V, radians
$C_{m_q} + C_{m_{\dot{\alpha}}}$, rad^{-1}	2	—		6	—	10	—	-5.5	0.2	0.3	0	0.049
	1	—		2	—	4	—	-5.4	0.6	1.7	0	0.017
	1	—		2	—	4	—	-5.8	0.9	1.7	0	0.012
	2	—		1	—	5	—	-5.8	0.9	1.7	0	0.006
	1	—		2	—	4	—	-4.9	1.1	1.7	0	0.010
	1	—		2	—	4	—	-5.3	1.3	1.8	0	0.009
$C_{m_{\dot{\alpha}}}$, rad^{-1}	13	—		2	—	28	—	0.075	0.6	1.7	0	0.017
	7	—		1	—	15	—	-0.040	0.9	1.7	0	0.012
	6	—		2	—	14	—	-0.031	1.1	1.7	0	0.010
	3	—		2	—	8	—	-0.029	1.3	1.8	0	0.009
C_m	3	—		12	—	18	—	0.008	0.2	0.3	20	0.049
	1	—		2	—	4	—	0.012	0.6	1.7	20	0.017
	1	—		1	—	3	—	-0.023	0.9	1.7	12	0.012
	1	—		1	—	3	—	-0.021	1.1	1.7	12	0.010
	1	—		1	—	3	—	-0.067	1.3	1.8	19	0.009
ωD/2V, rad	—	7.1×10^{-4}		—	2.8×10^{-3}	—	4.2×10^{-3}	0.049	0.2	0.3	---	---
	—	2.2×10^{-5}		—	1.7×10^{-4}	—	2.1×10^{-4}	0.017	0.6	1.7	---	---
	—	4.5×10^{-6}		—	6.0×10^{-5}	—	6.9×10^{-5}	0.006	0.9	1.7	---	---
	—	8.3×10^{-6}		—	1.1×10^{-4}	—	1.3×10^{-4}	0.012	0.9	1.7	---	---
	—	5.5×10^{-6}		—	9.0×10^{-5}	—	1.0×10^{-4}	0.010	1.1	1.7	---	---
	—	4.5×10^{-6}		—	7.9×10^{-5}	—	8.8×10^{-5}	0.009	1.3	1.8	---	---

*Abernethy, R. B. et al. and Thompson, J. W. "Handbook Uncertainty in Gas Turbine Measurements," AEDC-TR-73-5 (AD 755356), February 1973.

APPENDIX A
SUGGESTED STING CRITERIA[a]

Models	Model Regime	Mach Number	Measurements	Boundary Layer[b]	Critical Sting Length L_{cr}/D
Slender-flat-base cones	Subsonic	0.2 → <0.9	PB, C_A[d]	Turbulent	2.5
		0.2 → <0.9	C_m, C_N[e]	Turbulent	2[c]
		0.2 → <0.9	$C_{m_q} + C_{m_{\dot{\alpha}}}$	Turbulent	2
	Transonic	0.9 → 1.3	PB, C_A[d]	Turbulent	3
		0.9 → 1.3	C_m, C_N[e]		2
		0.9 → 1.3	$C_{m_q} + C_{m_{\dot{\alpha}}}$		2

Notes:

[a] Criteria for $\alpha = 0$ for PB, C_A, $C_{m_q} + C_{m_{\dot{\alpha}}}$

[b] Boundary layer condition generally at model base

[c] Possible; within the range $2.0 \leq L_{cr}/D \leq 3.3$

[d] PB measurements are also applicable to the calculation of C_A (which was not measurered)

[e] C_m measurements are also applicable to the calculation of C_N (which was not measurered)

APPENDIX B
THE PARAMETER $\Delta^i C_{m_\alpha}$

Section 3.4 explains why the static stability derivative, C_{m_α}, was not presented in this report. However, the parameter $\Delta^i C_{m_\alpha}$ was found to be representative of the measurement of C_{m_α} in determining critical sting length. The parameter $\Delta^i C_{m_\alpha}$ is defined as the difference between C_{m_α} for the clean sting configuration ($L_S/D \geq 3$) and C_{m_α} for any particular L_S/D. The effective sting-length configuration changes were made in such a way that the sting oscillation corrections and the model tare damping were not altered (see Section 2.2). Since $\Delta^i C_{m_\alpha}$ is a difference between two measurements having relatively the same sting oscillation correction, the sting oscillation effects are effectively removed. Thus, $\Delta^i C_{m_\alpha}$ is a measure of the aerodynamic change in the static stability derivative due to interference, but it cannot be used to depict the actual static stability characteristics of the model.

NOMENCLATURE

A	Reference area [based on model base diameter (D)], 0.349 ft^2
A/D	Analog-to-digital
AMAPS	Automatic Model Attitude Positioning System
C_A	Forebody axial-force coefficient, forebody axial force/Q • A
C_N	Normal-force coefficient, normal force/Q • A
C_m	Pitching-moment coefficient, pitching moment/Q • A • D
C_{m_q}	Pitching-moment coefficient due to pitch velocity, $\partial_m/\partial(qD/2V)$, $radian^{-1}$
C_{m_α}	Pitching-moment coefficient due to angle of attack, $\partial C_m/\partial\alpha$, $radian^{-1}$
$C_{m_{\dot\alpha}}$	Pitching-moment coefficient due to rate of change of angle of attack, $\partial(C_m)/\partial(\dot\alpha D/2V)$, $radian^{-1}$
D	Reference length (model base diameter), 0.667 ft
D_S	Sting diameter at model base, in.
L_{cr}	Critical sting length, in. (for $L_S < L_{cr}$, model data are affected)
L_S	Effective sting length (from model base to sting flare, see Fig. 2), in.
M	Free-stream Mach number
OC	Oscillatory component
P	Free-stream static pressure, psf
PB	Model base pressure, psf
PT	Tunnel stilling chamber pressure, psfa
q	Pitching velocity, radian/sec
Q	Free-stream dynamic pressure, psf
Re_D	Free-stream Reynolds number based on reference length (D)
SC	Static component
TT	Tunnel stilling chamber temperature, °R

V	Free-stream velocity, ft/sec
α	Angle of attack, deg or radians
$\dot{\alpha}$	Time rate of change of angle of attack, radian/sec
$\Delta^{I}C_{m_{\alpha}}$	Incremental change in $C_{m_{\alpha}}$ due to interference (see Appendix B for definition), radian^{-1}
θ	Oscillation amplitude, deg
θ_s	Flare angle of sting (see Fig. 2), deg
ω	Oscillation frequency, radian/sec
$\omega D / 2 V$	Reduced frequency parameter, radian